Visualization of Fuel Cell Water Transport and Performance Characterization Under Freezing Conditions

RIT: Satish Kandlikar (PI), Zijie Lu

GM: Jon Owejan, Jeffrey Gagliardo, Thomas Trabold

MTU: Jeffrey Allen, Reza Shahbazian-Yassar

June 8, 2010

Project ID #: FC056

Overview

Timeline

- Start date: 03/01/2007
- End date: 02/28/2010
- Status: Completed

Barriers

- Barriers addressed
  C. Performance
  D. Water Transport within the Stack
  E. Thermal System and Water Management

Budget

- Total project funding
  - DOE: $ 2.68M
  - Contractor: $ 0.8M

- FY07: $ 0.9M
- FY08: $ 0.9M
- FY09: $ 0.9M

Partners

- Interactions/ collaborations
  - Rochester Institute of Technology
  - General Motors Corporation
  - Michigan Technological University
- Project lead:

  Rochester Institute of Technology

Objectives - Relevance

- Improve fundamental understanding of the water transport processes under freezing and non-freezing conditions.

- To minimize fuel cell water accumulation while suppressing regions of dehumidification by an optimized combination of
  - New gas diffusion layer (GDL) material and design,
  - New bipolar plate (BPP) design
  - Surface treatment
  - Anode/cathode flow conditions.

- To meet DOE 2010 targets for 80 kWe transportation stacks:

Start up and shut down energy from -20°C ambient	Unassisted start temperature	Cold start-up time to 50% of rated power @ –20ºC ambient
5 MJ	**- 40 °C**	**30 s**

Approach and Project Milestones

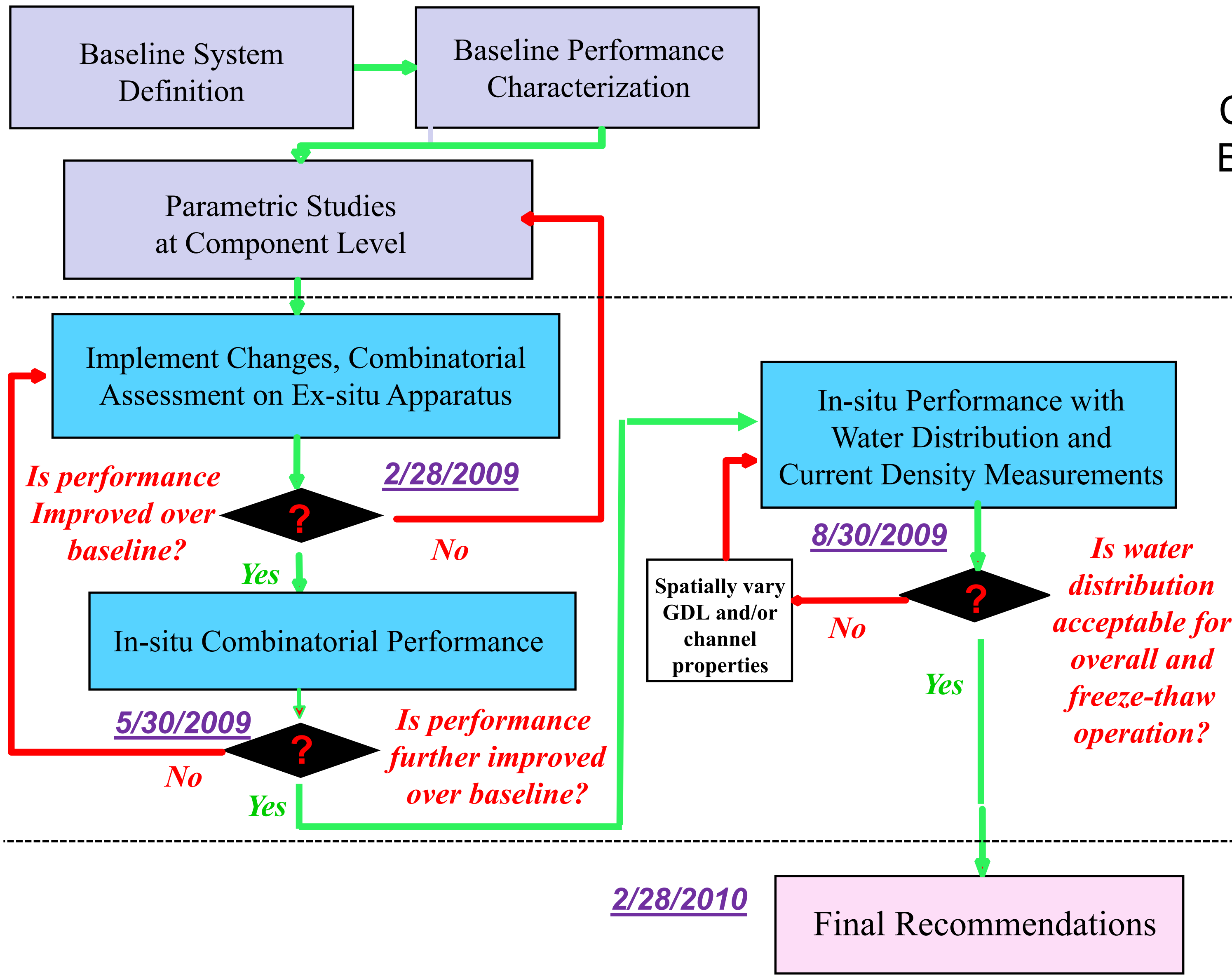

Phase I:

Characterize the Baseline System

Phase II:

Implement changes to baseline system and assess the performance

Fuel Cell Design

Flow Channel Design

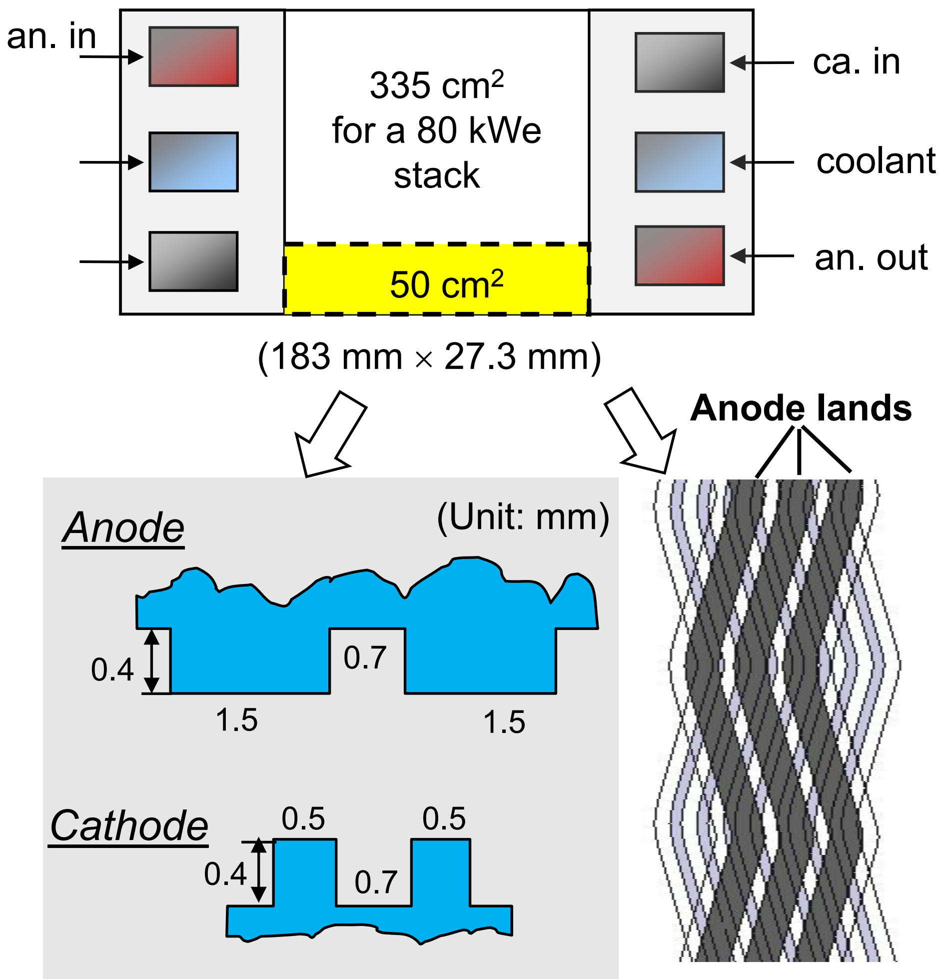

Test Section for Neutron Radiography

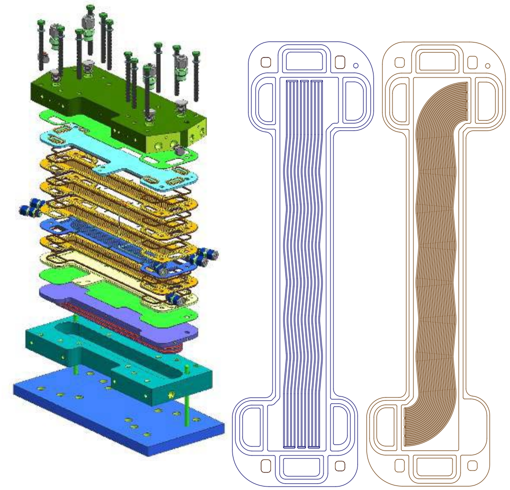

Test Section for Multichannel Flow Exp.

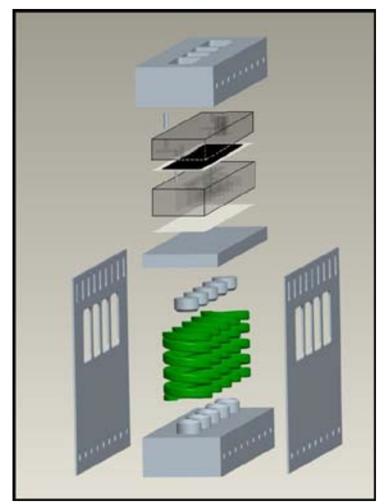

- The designed fuel cell meets DOE 2010 target of 2 kW/L.

Water Accumulation Correlated to Freeze Failure

Precondition: 0.4 A/cm2, 150 kPa, 35°C, A/C stoich = 2/2, Dry inlet gas
Purge: 0.1 A/cm2, 150 kPa, 35°C, A/C stoich = 2/12, Dry inlet gas

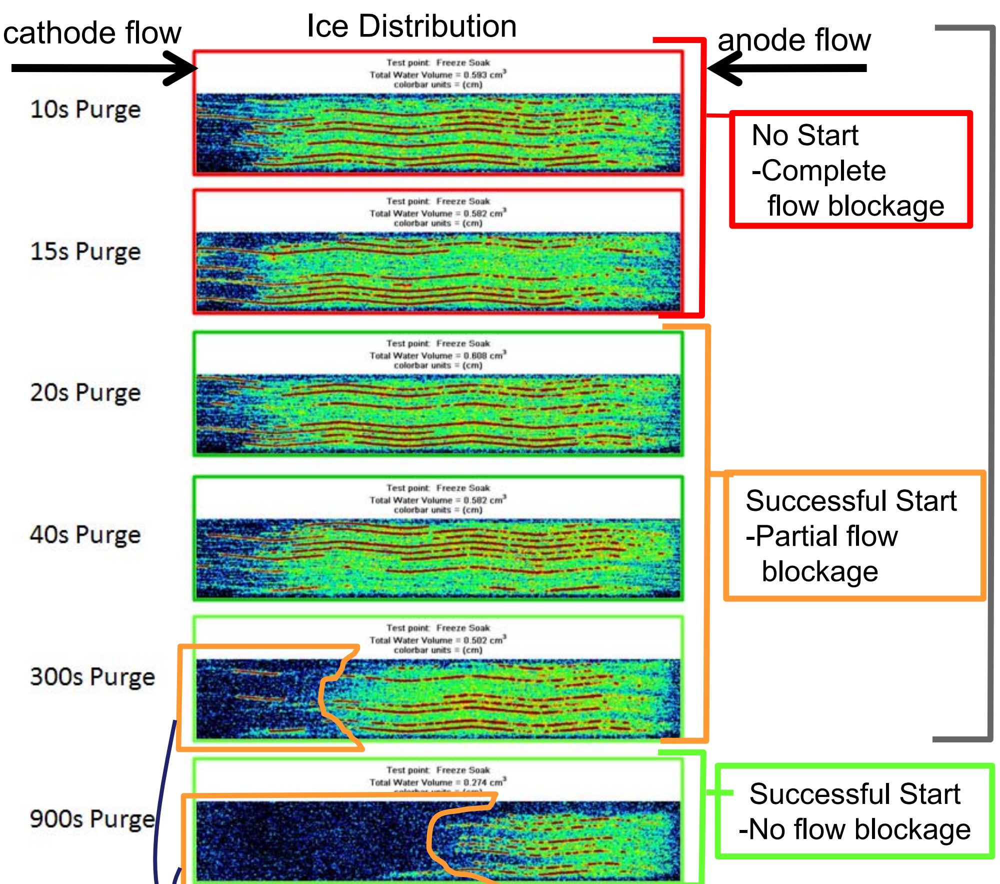

Evaporating water from porous layers extends run time while frozen, by providing space for additional ice formation and accumulation

Water Accumulation in the Exit Region and Headers

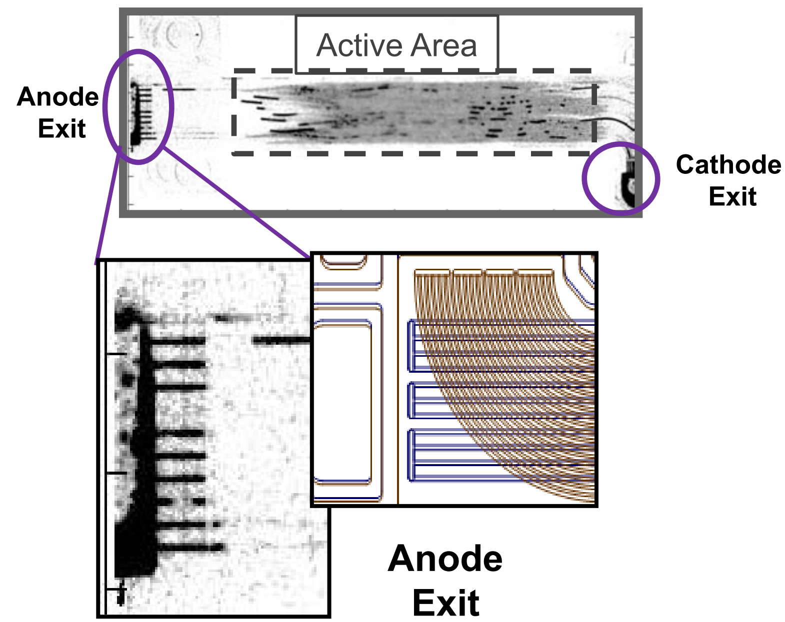

- Freeze failure is correlated to water accumulation within a fuel cell.
- Purge provides a viable method to mitigate the water accumulation.

Purge Water Removal Rate Characterization

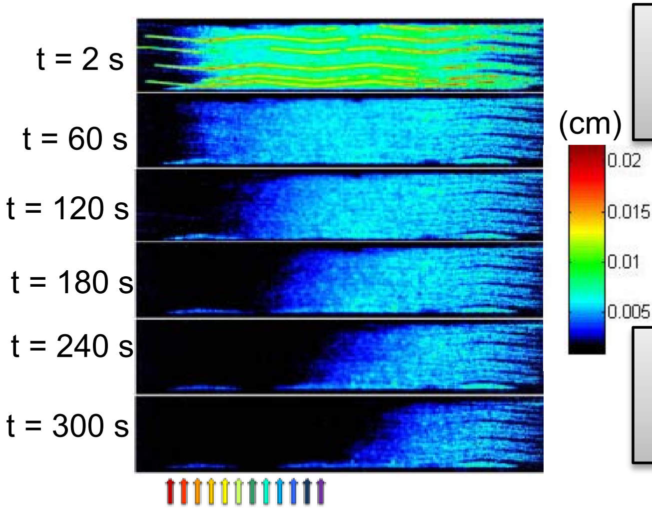

Precondition:
33°C, dry gas, 0.4 A/cm^2, 150 kPa

Purge:
100 kPa, 33°C, 1 SLPM dry N2

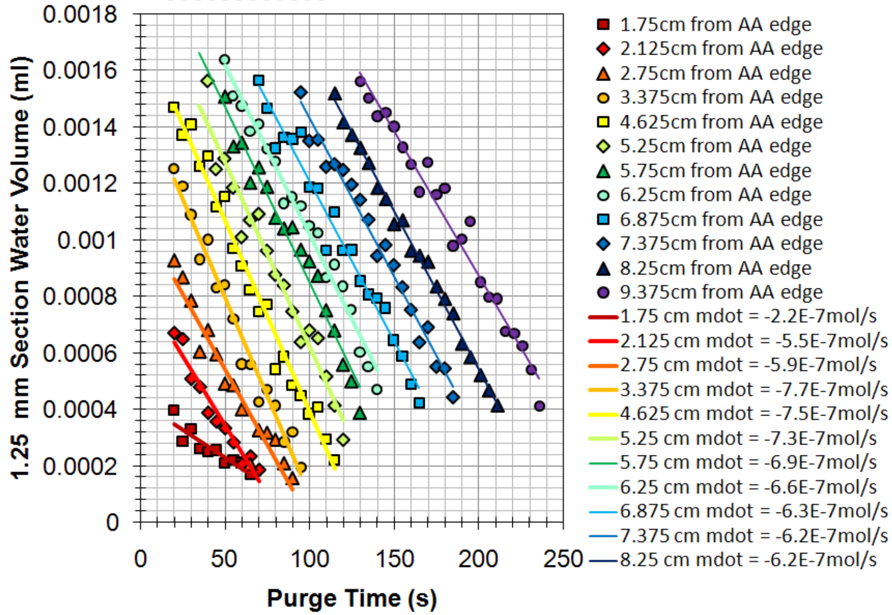

Ex-situ saturated with known water location

Temperature	Ex-situ Saturated GDL	Differential Removal Rate (μL/s)	Drying Front Length after 330 s purge (cm)
33°C	Cathode	0.0203 ± 0.0023	5.2 ± 0.3
33°C	**Anode**	0.0090 ± 0.0011	11.5 ± 0.3
76°C	Cathode	0.0758 ± 0.0076	15.7 ± 0.5
76°C	**Anode**	0.0283 ± 0.0017	>18.3

In-situ saturated with unknown water location

Temperature	Differential Removal Rate (μL/s)	Drying Front Length (cm)
33°C	0.010 ± 0.0011	10.8 ± 0.4
76°C	0.0281 ± 0.0037	>18.3

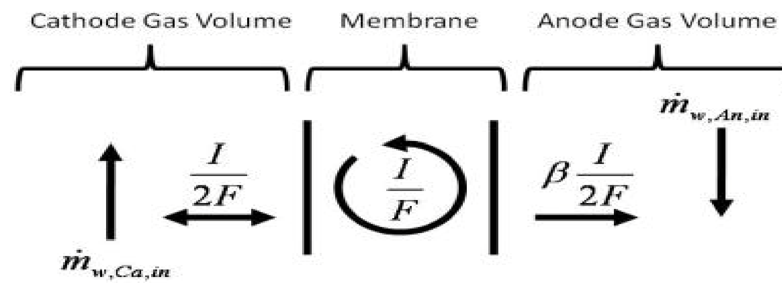

- For a cathode purge, liquid water accumulation in the anode GDL constrains the removal rate.

Constant Drying Rate Model for PEMFC Purge

Saturated gas at the GDL surface, Hc = constant

$$\frac{dm_w}{dt} = -KV_{GDL}\left(H_{GDL} - H_p\right) = -\frac{\dot{m}_p V_{GDL}}{A_{chan}}\frac{dH_p}{dx}$$

$$\left(\frac{\partial m_w}{\partial t}\right)_y = -KV_{GDL}(H_c - H_i)e^{-\frac{KA}{\dot{m}_p}y}$$

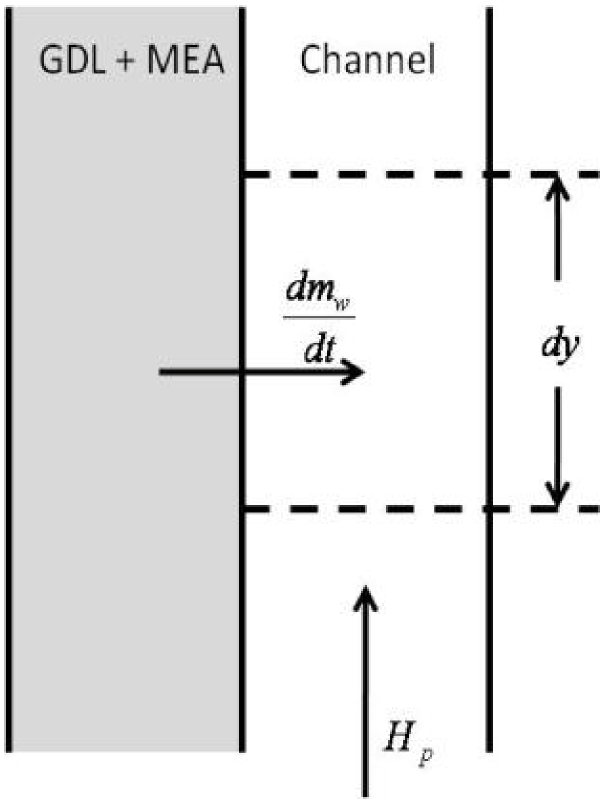

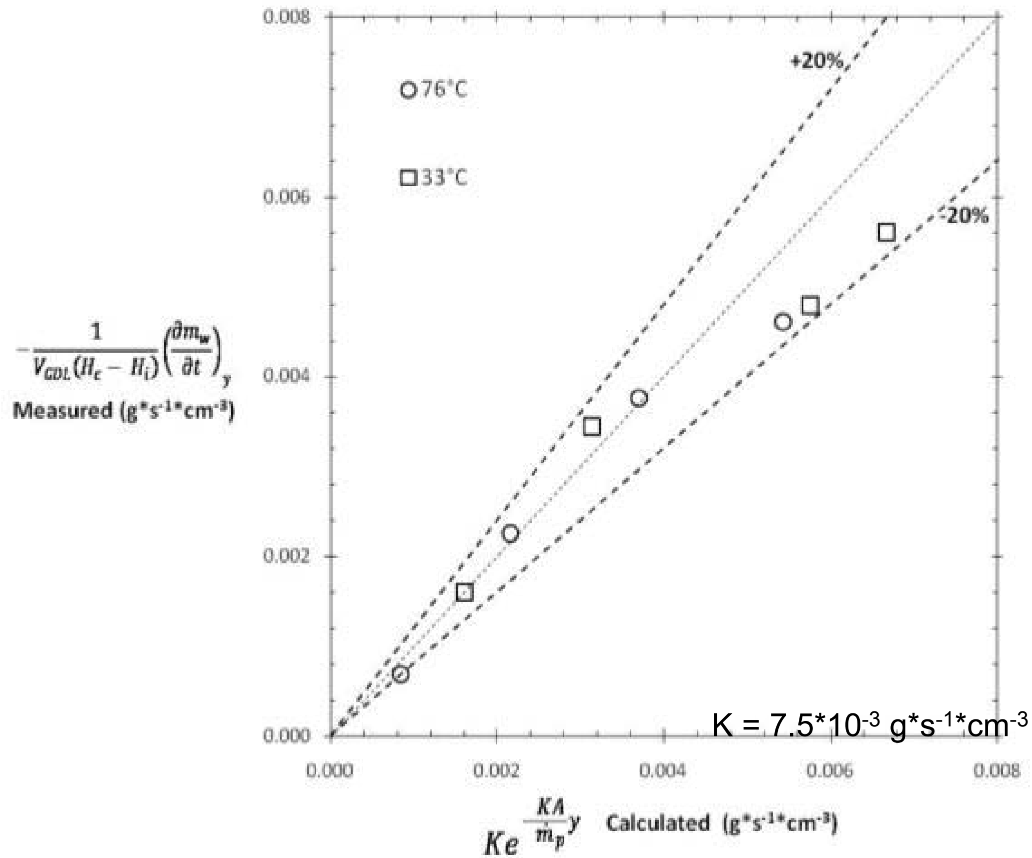

- So... If the initial saturation state is known, purge drying is easily predicted.

Simultaneous Water, Current, HFR, and Temperature Measurement

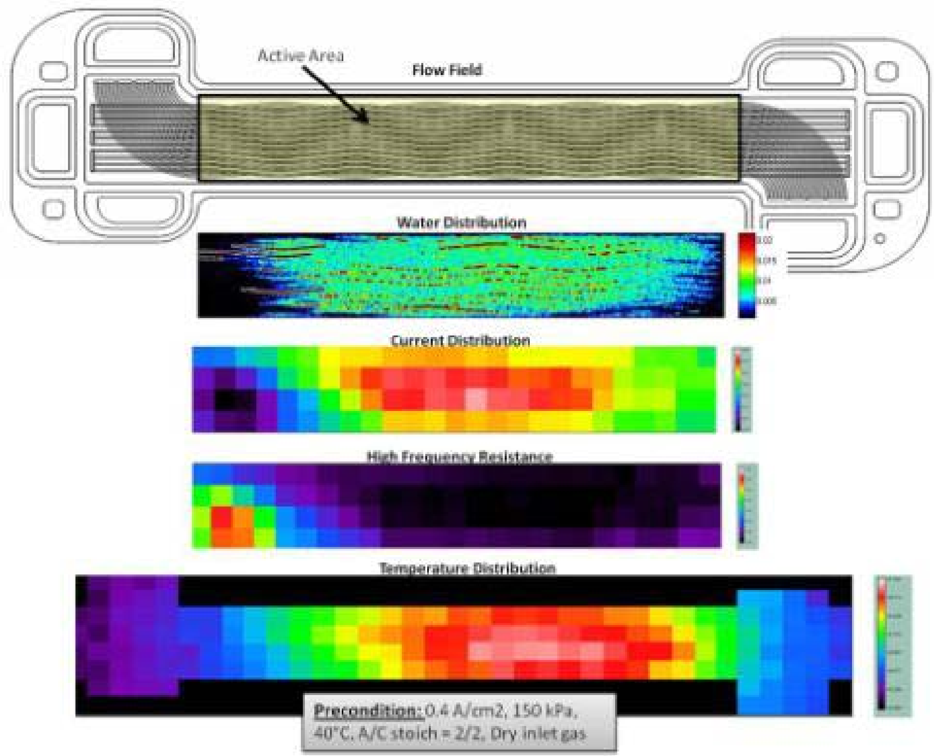

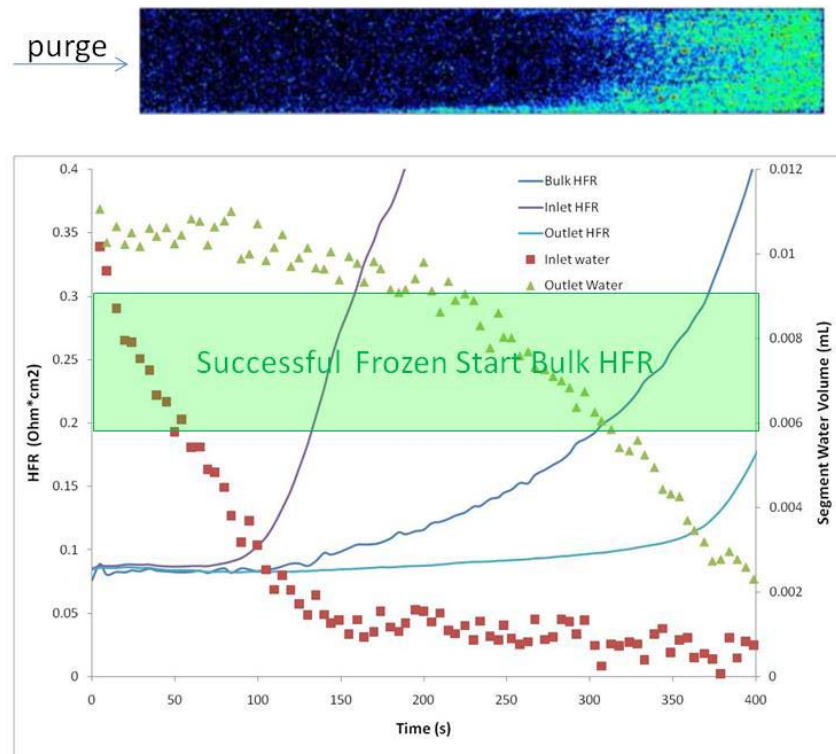

- ❑ Local temperature, current density and HFR vary significantly for a given precondition

- ❑ Bulk HFR measurement alone is not sufficient to optimize purge conditions and materials for successful starts. The relationship of local HFR increases with drying must be known.

Liquid Water Content and HFR

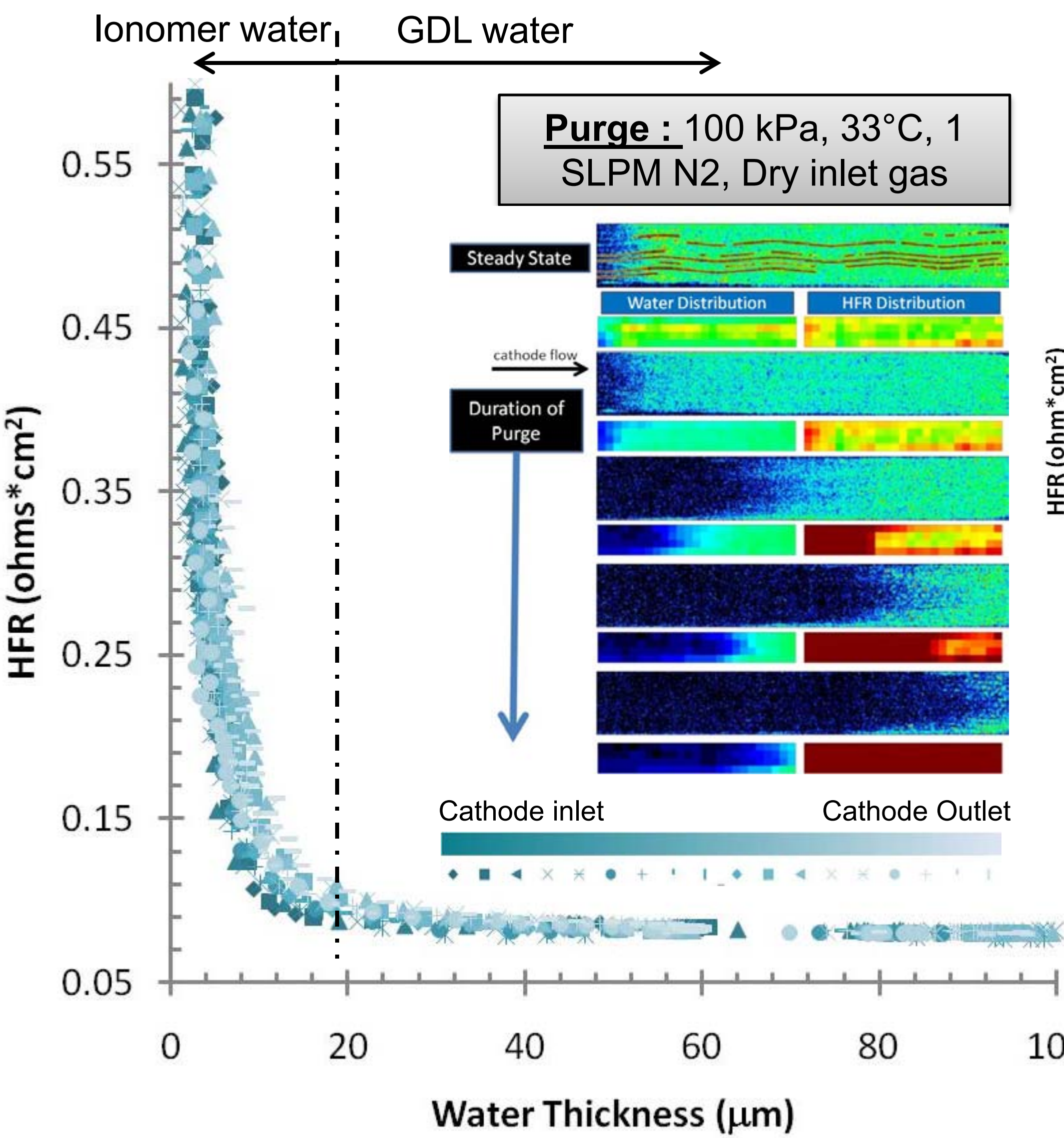

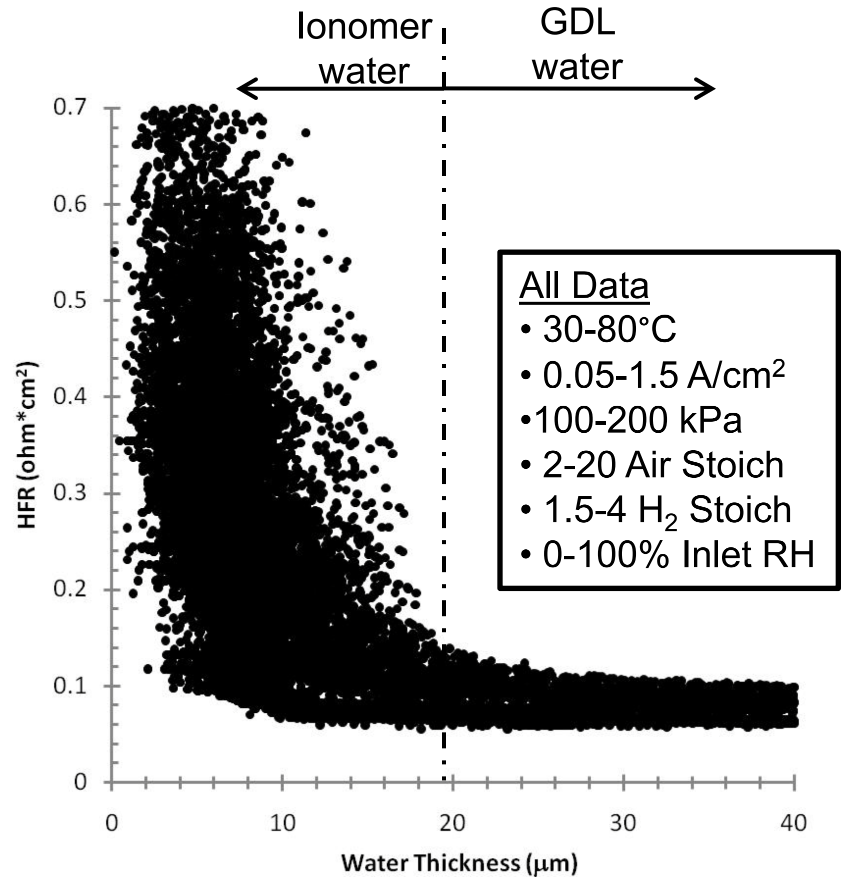

- ❑ Liquid water required in GDL to minimize HFR as transition is very sensitive.

Separating Impact of GDL Thermal Properties

Precondition:
33°C, dry inlet gases, 0.4 A/cm², 2/2 An/Ca Stoich, 150 kPa

@ 33°C

Lower thermal conductivity saturation

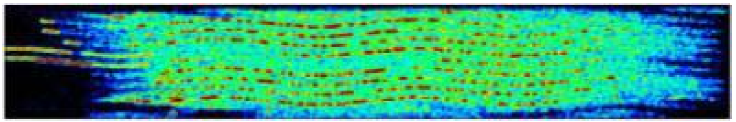

~

Higher thermal conductivity saturation

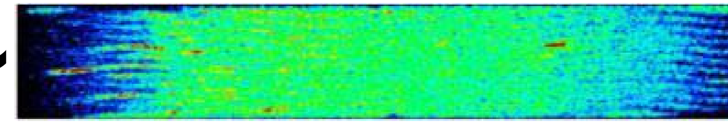

Precondition:
76°C, 95% RH inlet gases, 0.4 A/cm², 2/2 An/Ca Stoich, 150 kPa

@ 76°C

Lower thermal conductivity saturation

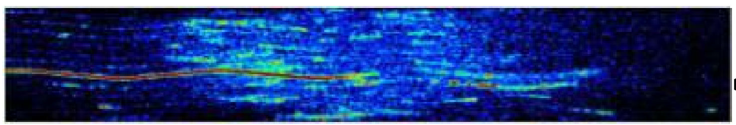

<

Higher thermal conductivity saturation

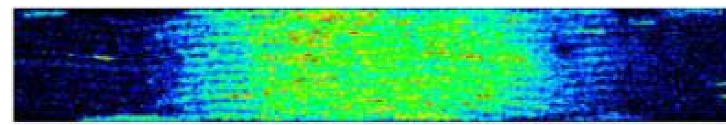

- ❑ The driving force for vapor transport is 10X higher at 76°C as compared to 33°C.

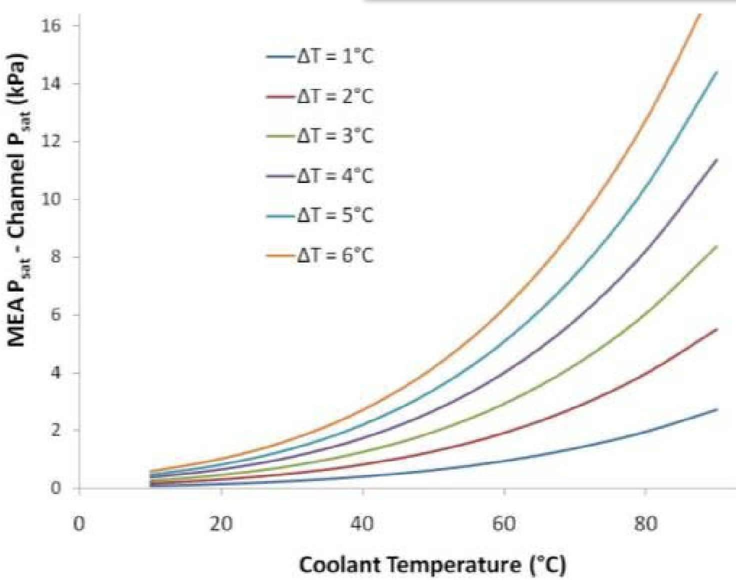

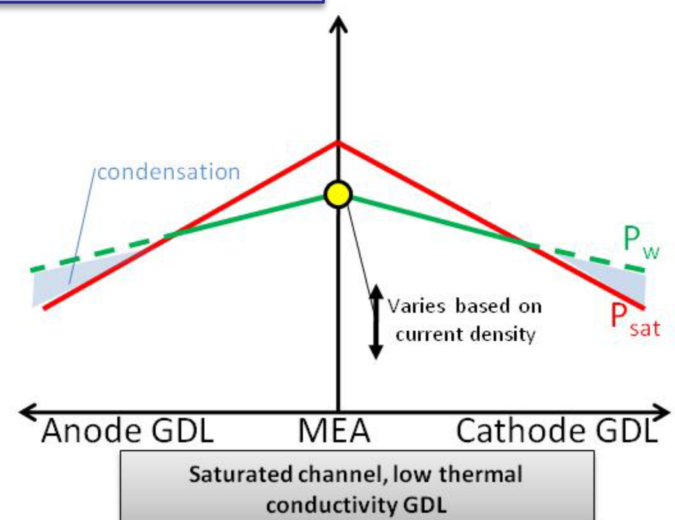

*Differential Flow Conditions in Channel

GDL Thermal Conductivity Impact on Water Accumulation

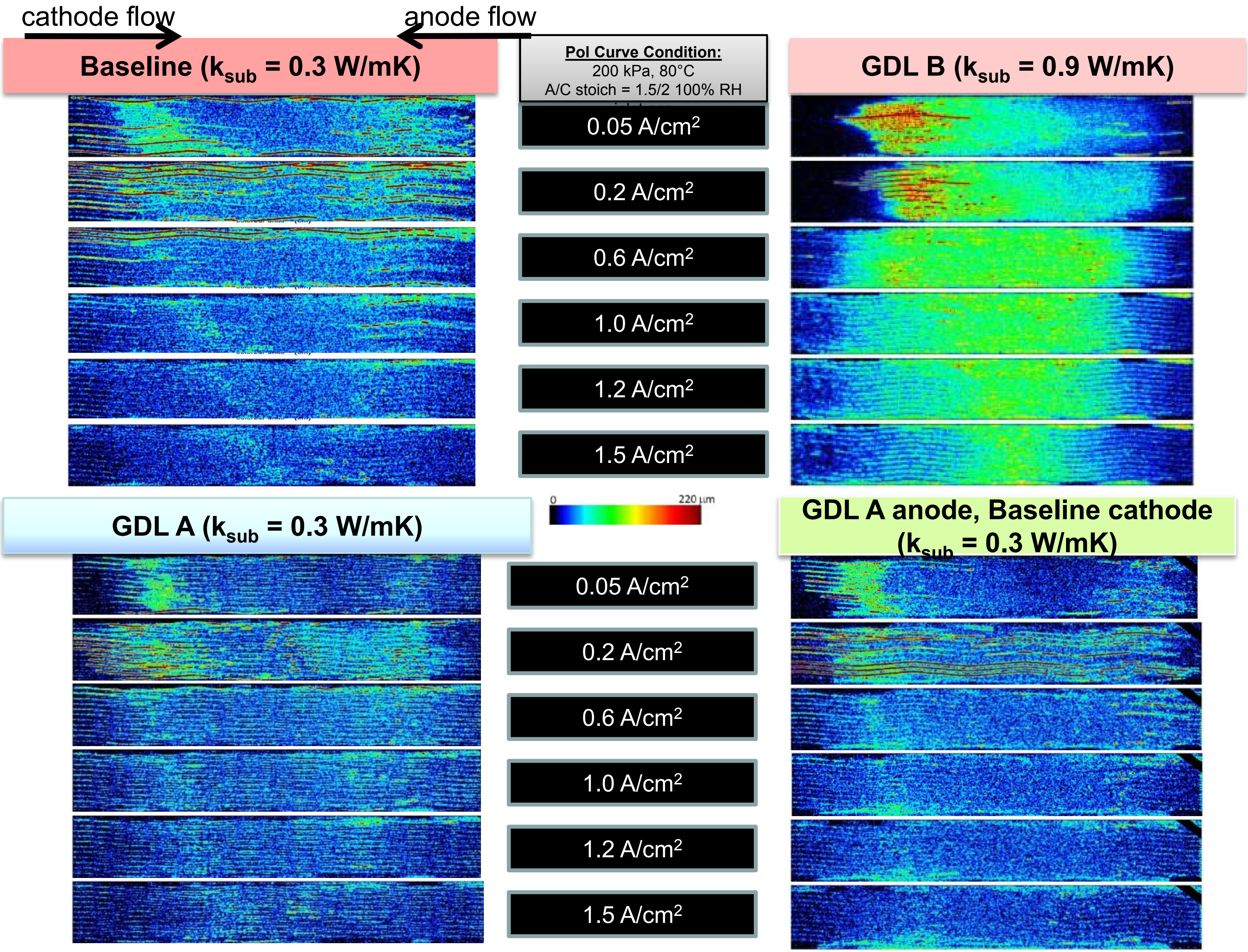

What Impacts the Initial Saturation State – GDL Thermal Conductivity?

Low heat flux = small temperature gradient, values should be similar

As heat flux increases, more conductive substrates have lower dT and more water condenses

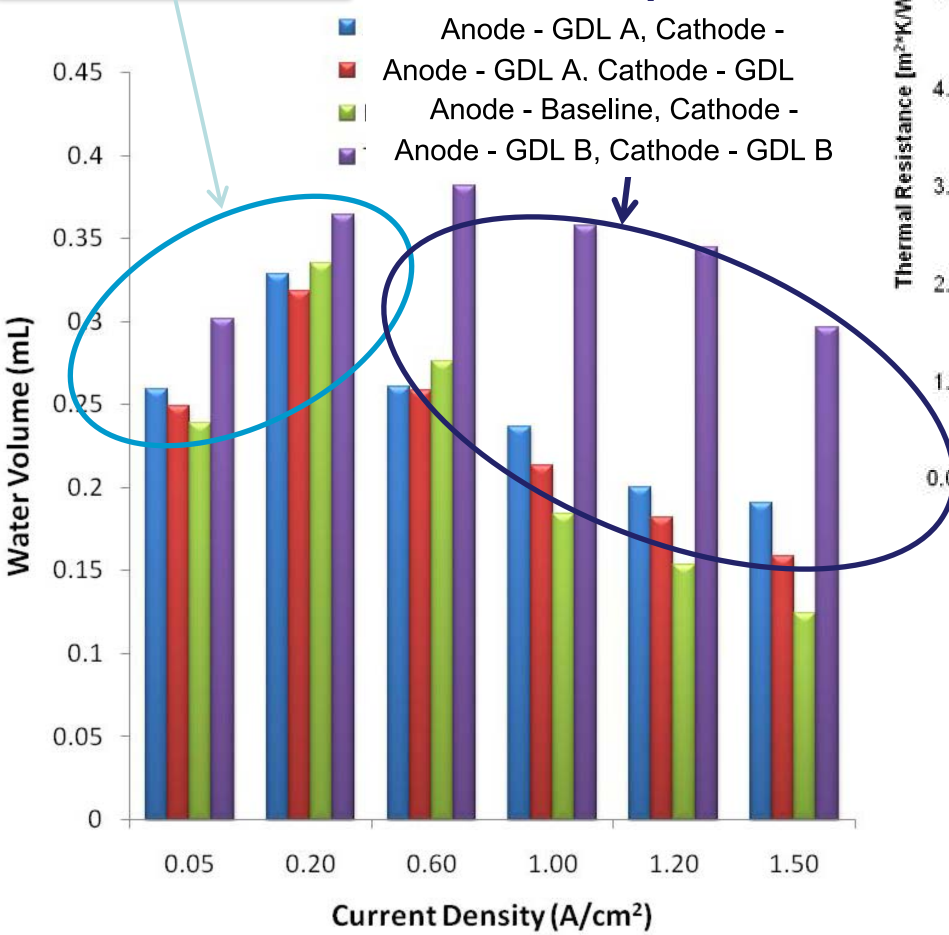

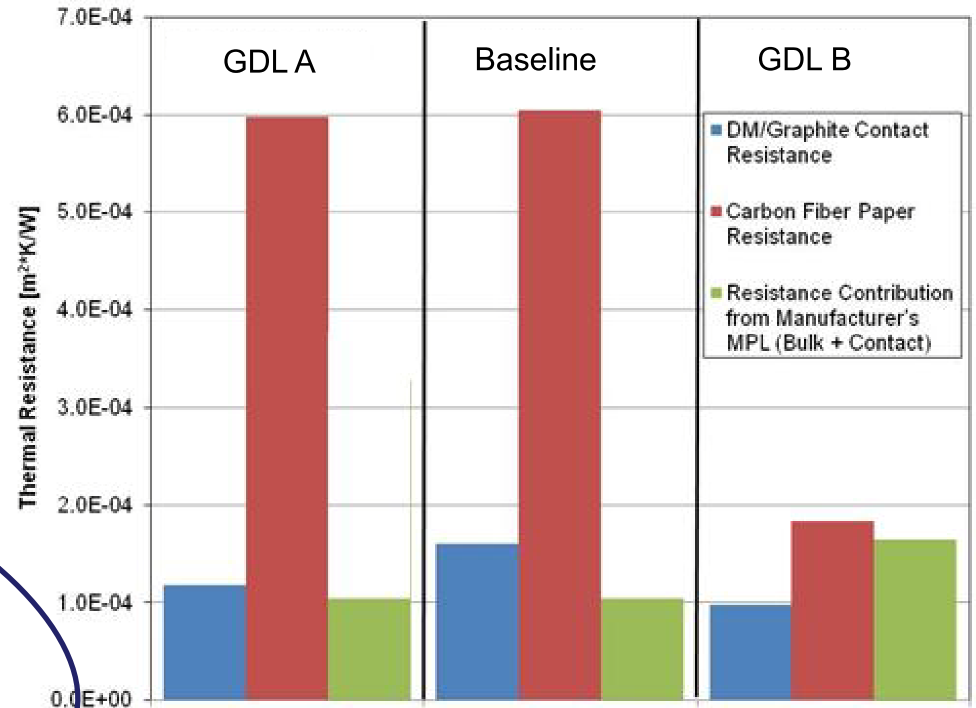

Higher thermal conductivity effectively lowers the saturation pressure near the MEA and more condensation in the bulk substrate results.

Verifying A Down-the-Channel Model From Experimental Data

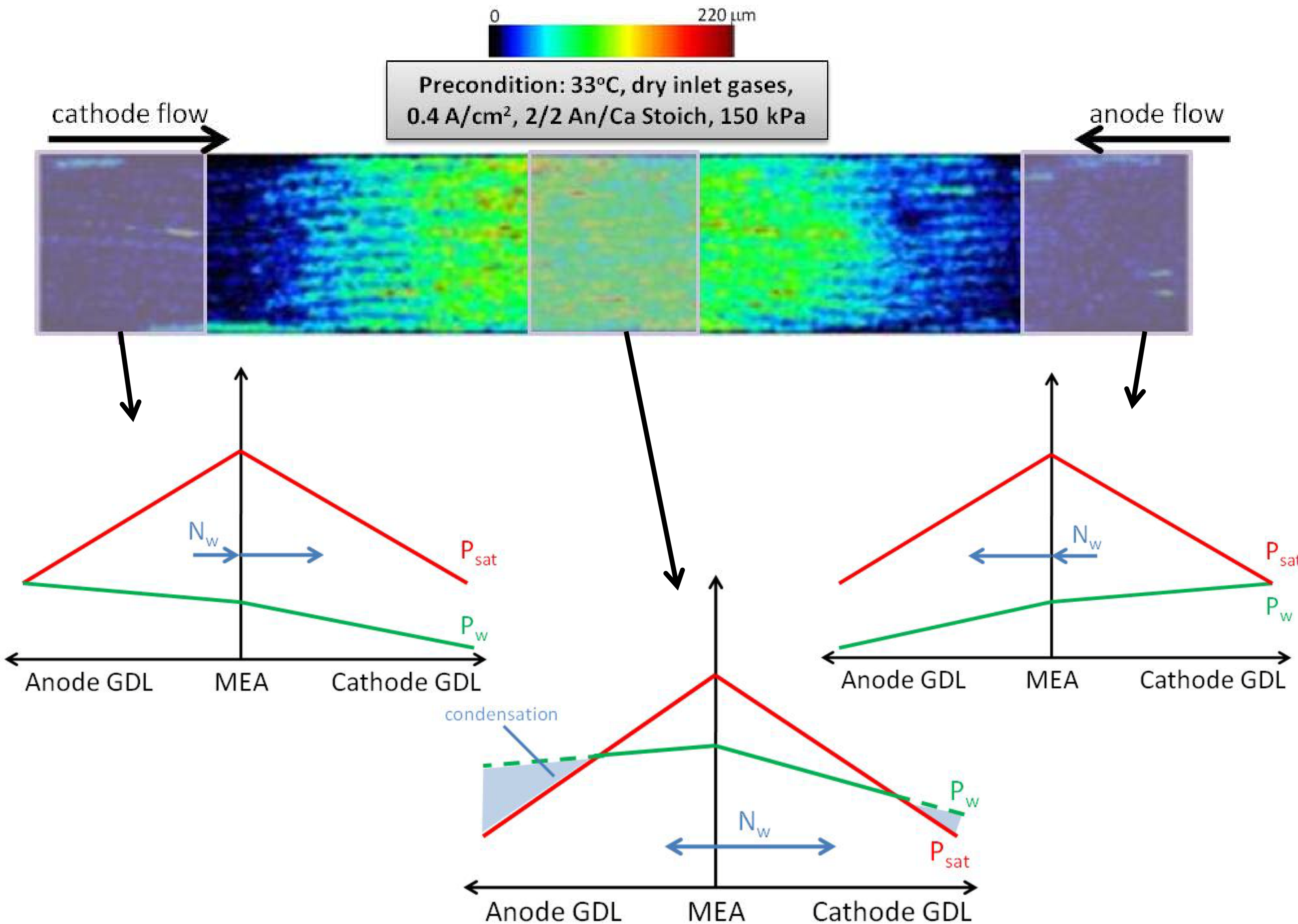

Through-Plane Location of Water Accumulation, Land vs. Channel

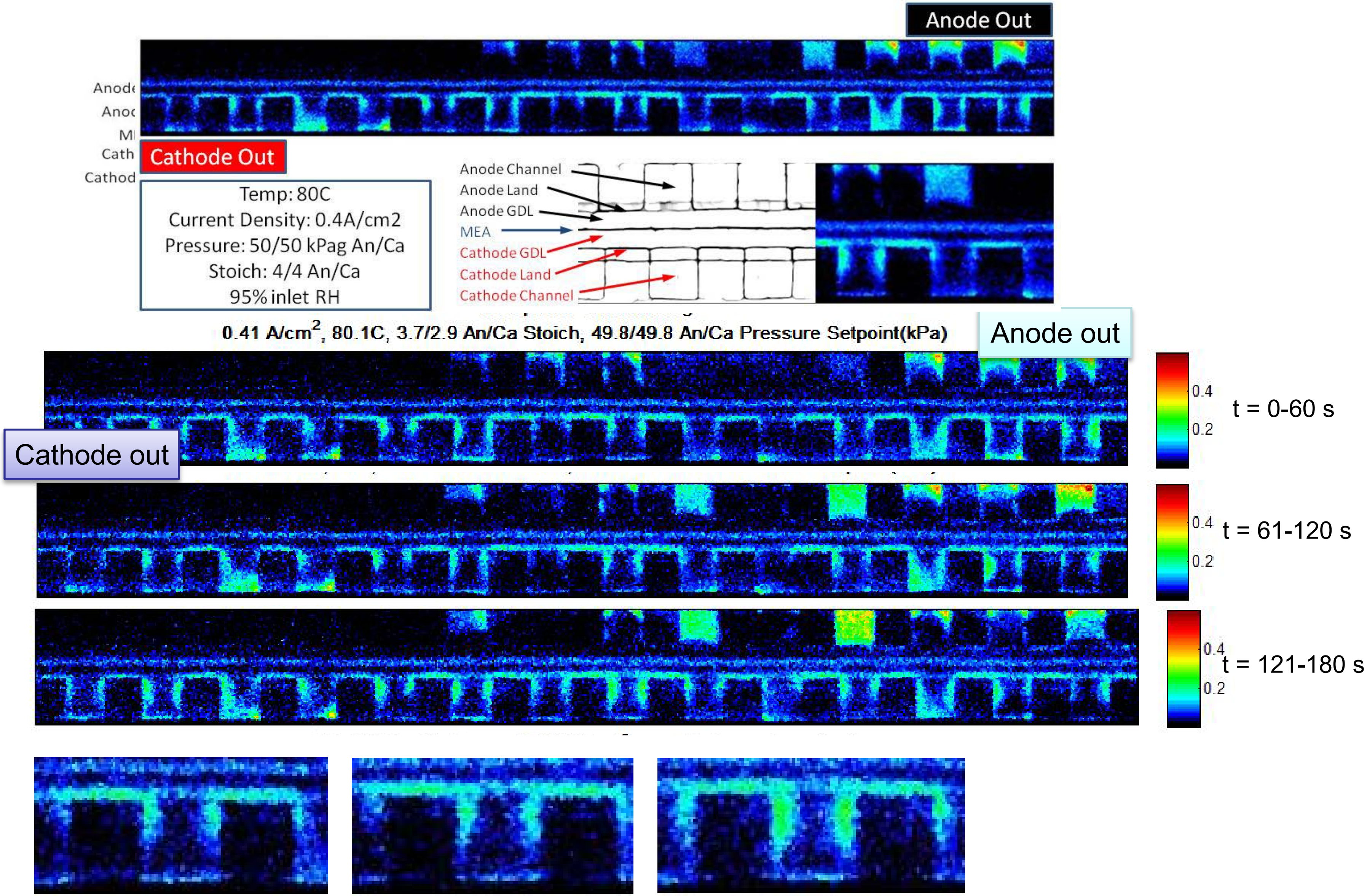

Down-the-Channel Variation in GDL Thermal Conductivity

cathode flow

Graded Anode GDL B + Baseline

anode flow

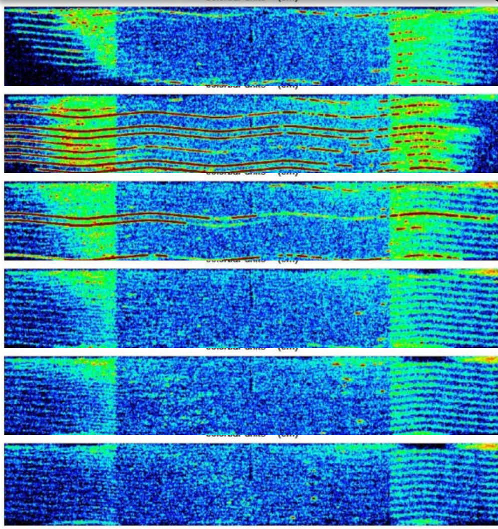

0.05 A/cm²

0.2 A/cm²

0.6 A/cm²

1.0 A/cm²

1.2 A/cm²

1.5 A/cm²

Baseline

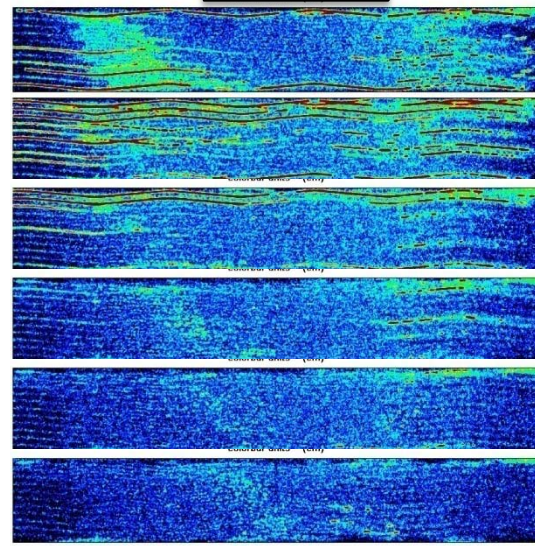

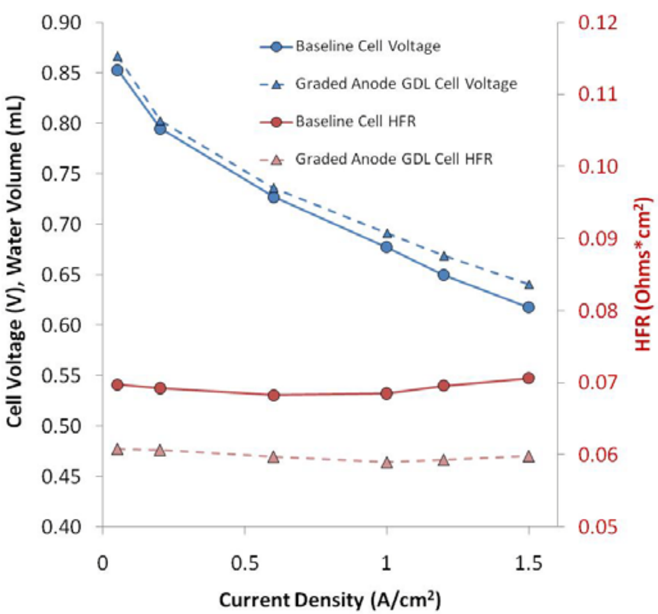

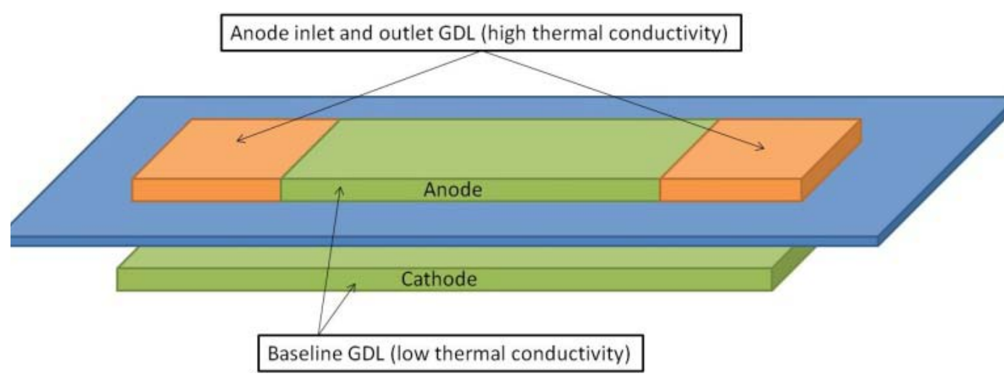

Water Transport in Channels - Flow Maldistribution

Entrance Region Pressure Drop Method:

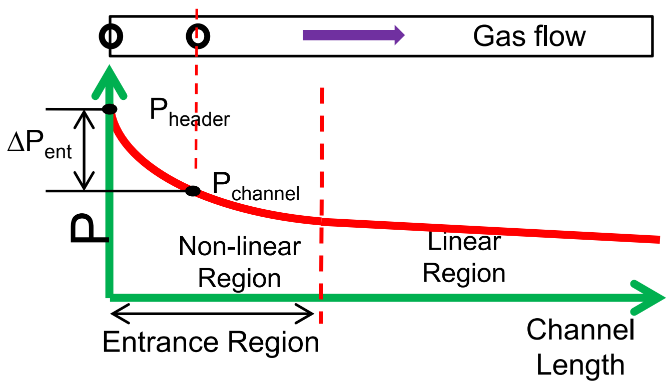

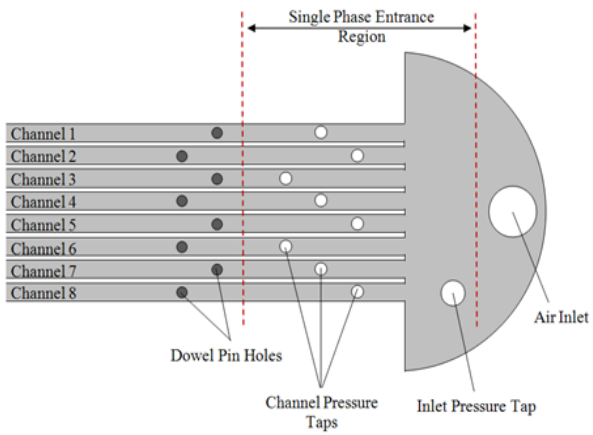

Ex-situ multi-channel exp.

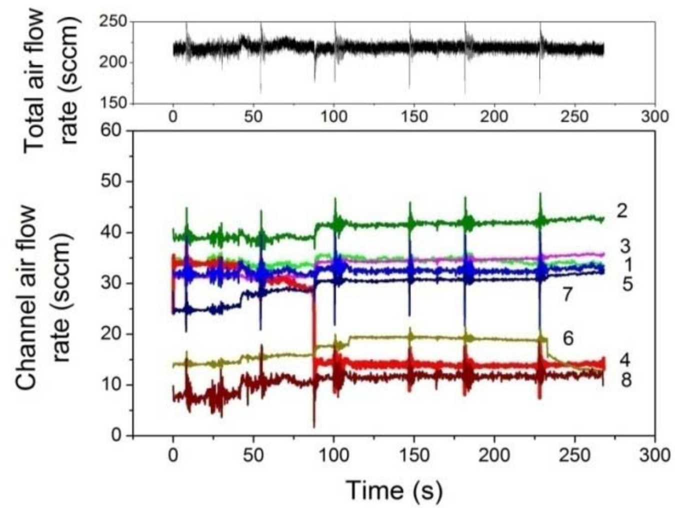

In-situ multi-channel exp.

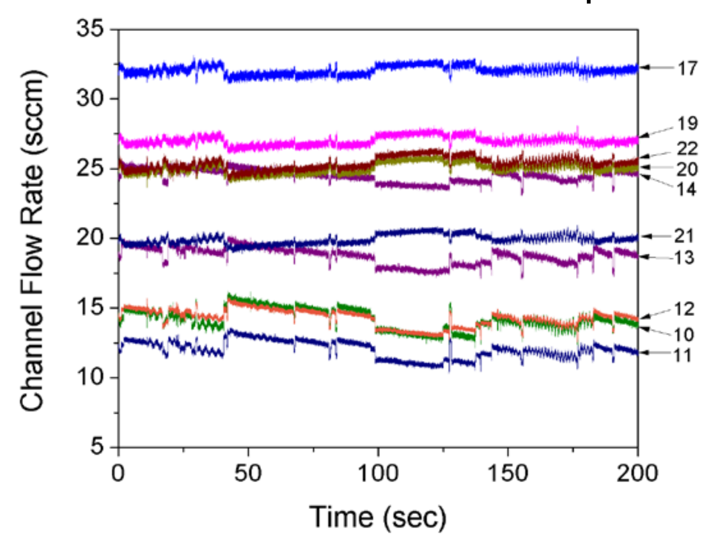

- ❑ Instantaneous flow distribution in individual channels measured.
- ❑ Water accumulation in channels is an important cause of flow maldistribution.

Non-uniform GDL Intrusion under Compression

- GDL intrusion quantified by three methods: Optical; Analytical; and CFD simulation (ANSYS)

Test section

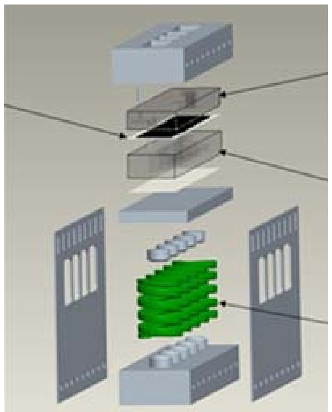

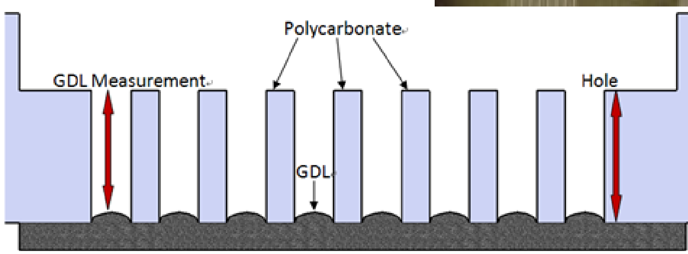

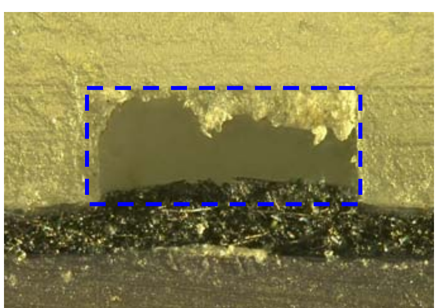

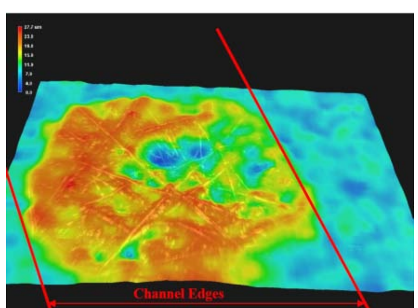

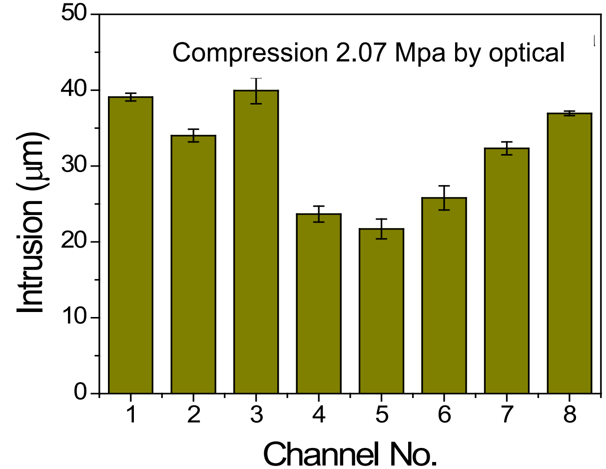

Intrusion effect on pressure drop

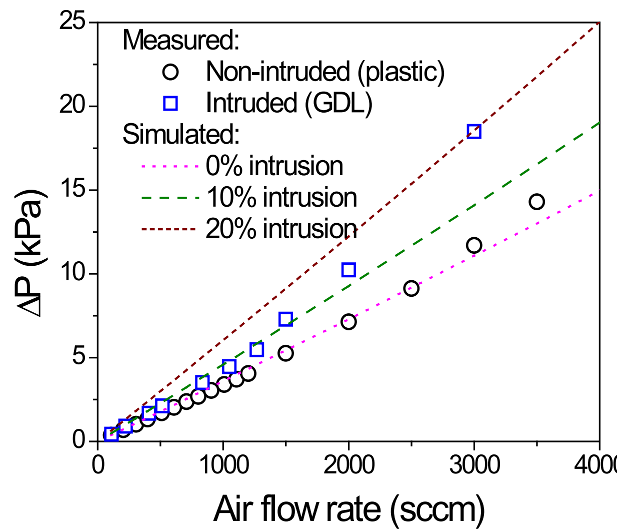

Channel Two-Phase Flow Characterization – Flow Pattern Map

Pressure drop signature

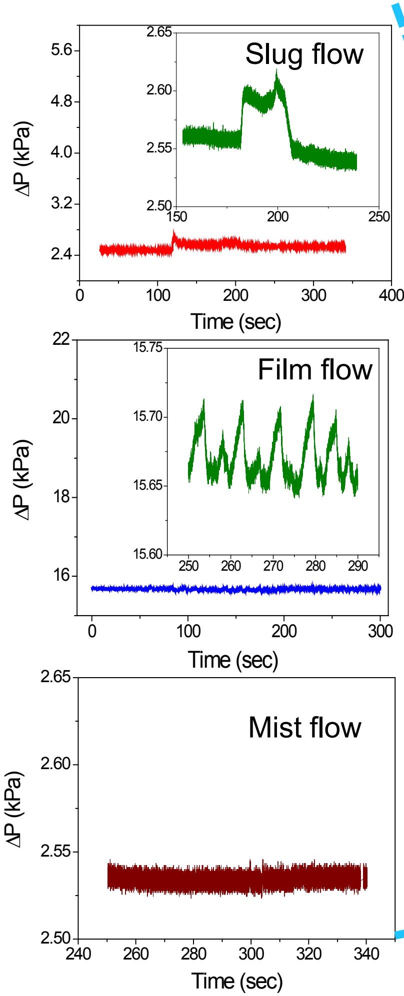

Visualization

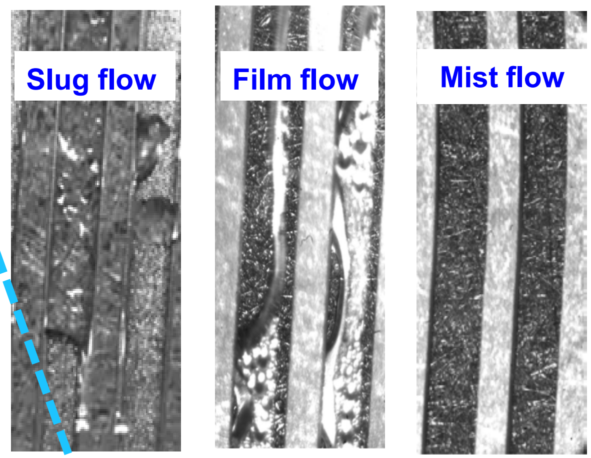

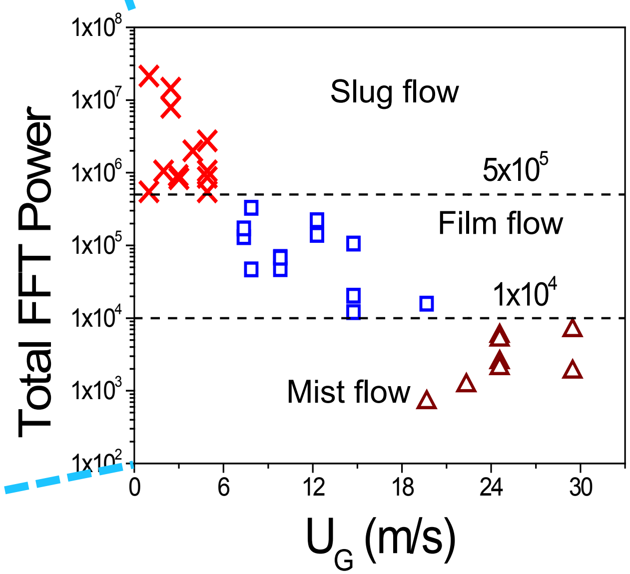

Ex-situ Flow Pattern Map

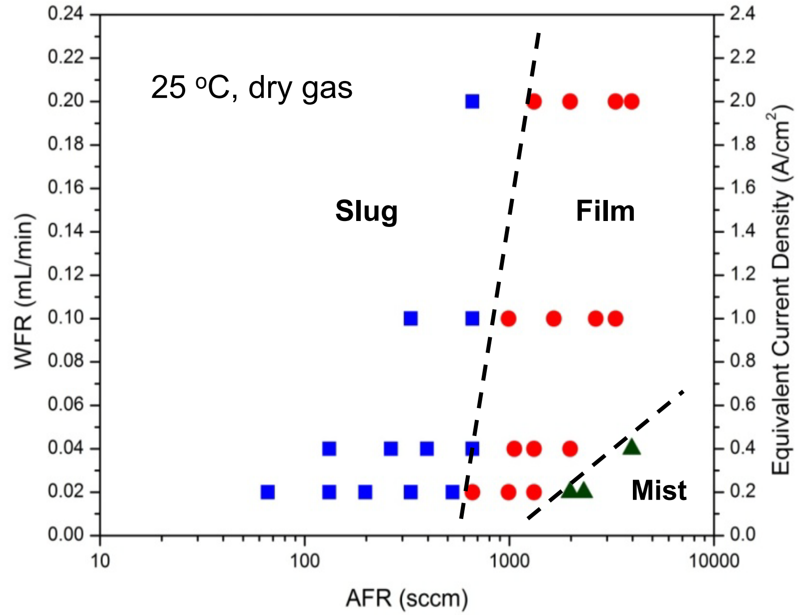

- Three basic flow patterns: Slug, Film, Mist
- Flow pattern map is identified as the key parameter in the performance matrix.

Improvement of Channel Water Removal – Hydrophilic Channel Surface

Non-treated channel ($\theta \sim 75^o$)

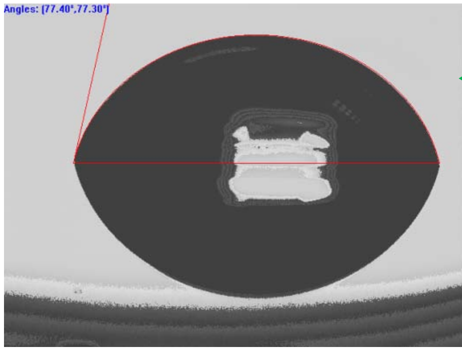

Non-treated channel – vapor polished Lexan

Hydrophilic channel ($\theta \sim 11^o$)

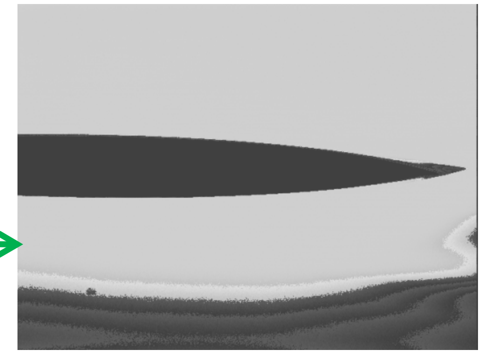

Hydrophilic channel – coated on the non-treated channel

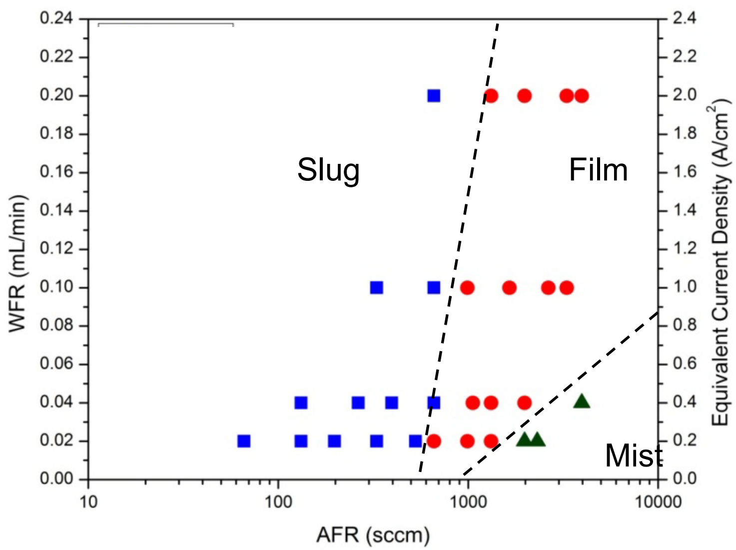

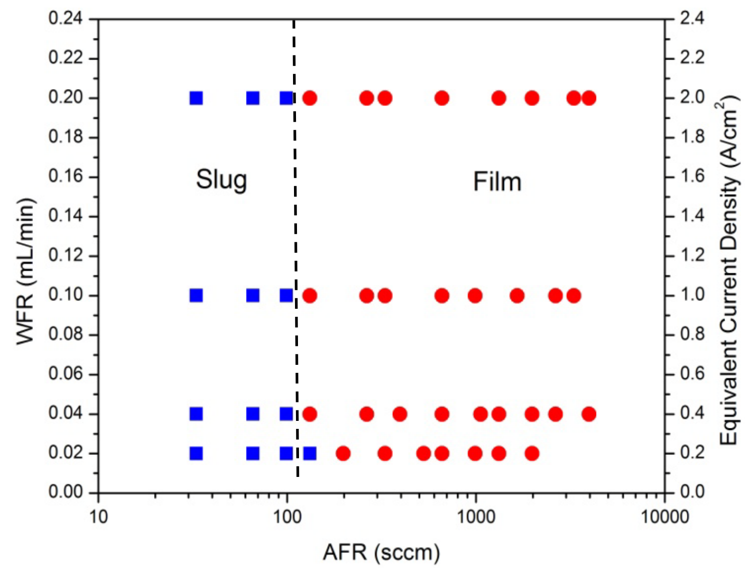

- Hydrophilic channels have a smaller slug region and are mostly film dominant, showing better water transport dynamics in gas channels.

Implement New Channel Geometries

Channel Geometries	Dimensions	D_h (mm)	**Slug flow** WFR = 0.4 mL/min AFR = 264 sccm	**Film flow** WFR = 0.4 mL/min AFR = 1057 sccm
Rectangular (Idealized)	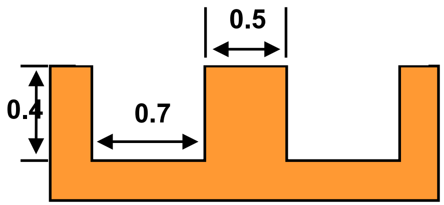	0.51	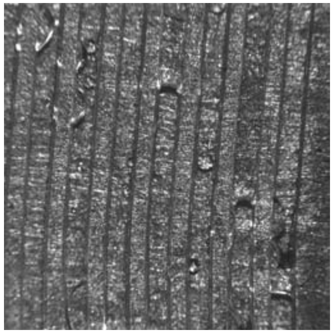	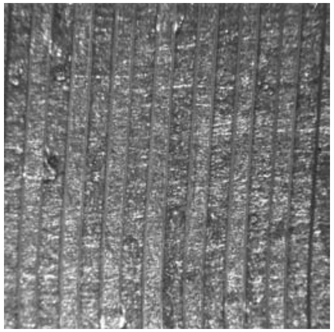
Sinusoidal (stamped metal)	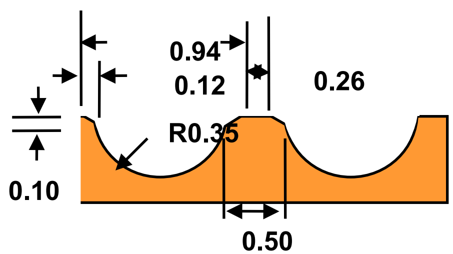	0.47	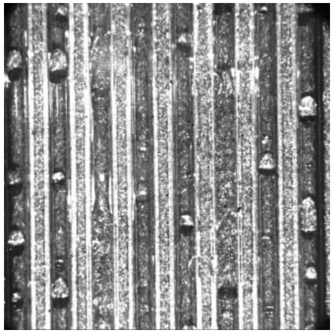	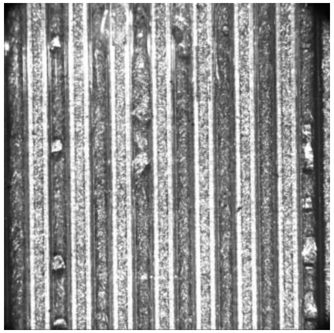
Trapezoidal (Molded composite)	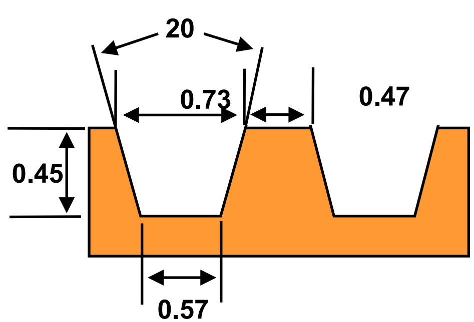	0.53	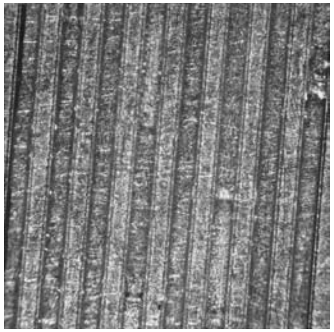	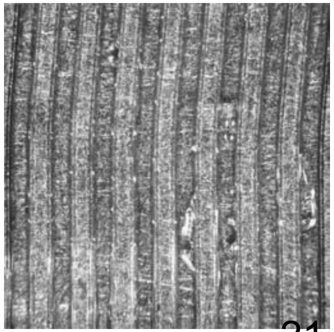

Effect of Channel Geometries on Flow Pattern Map

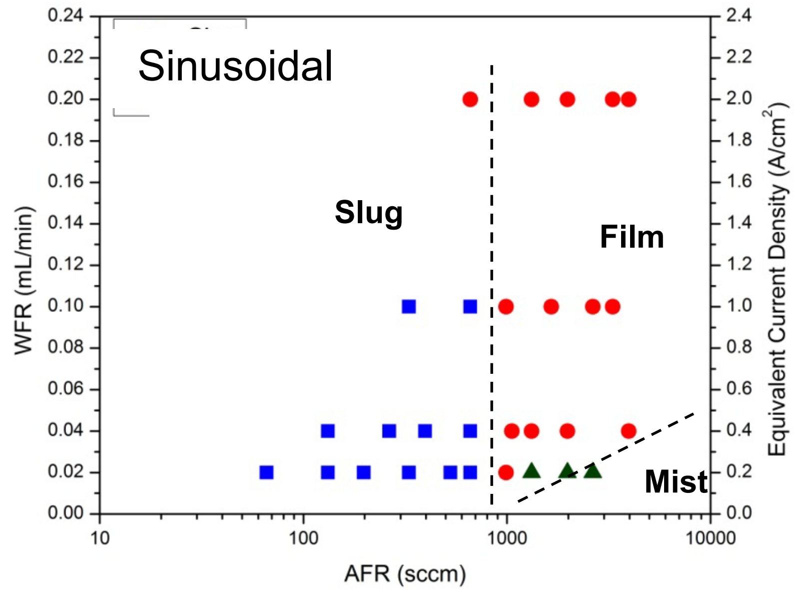

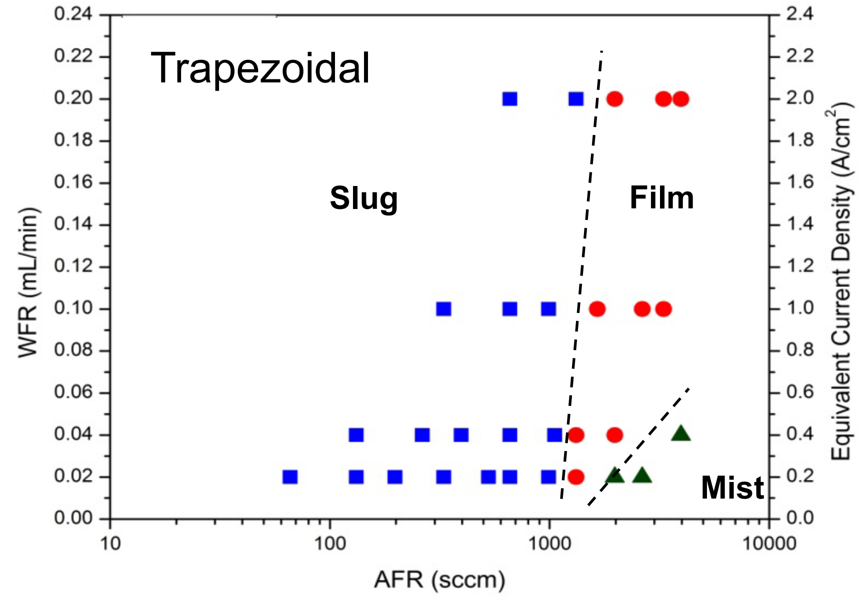

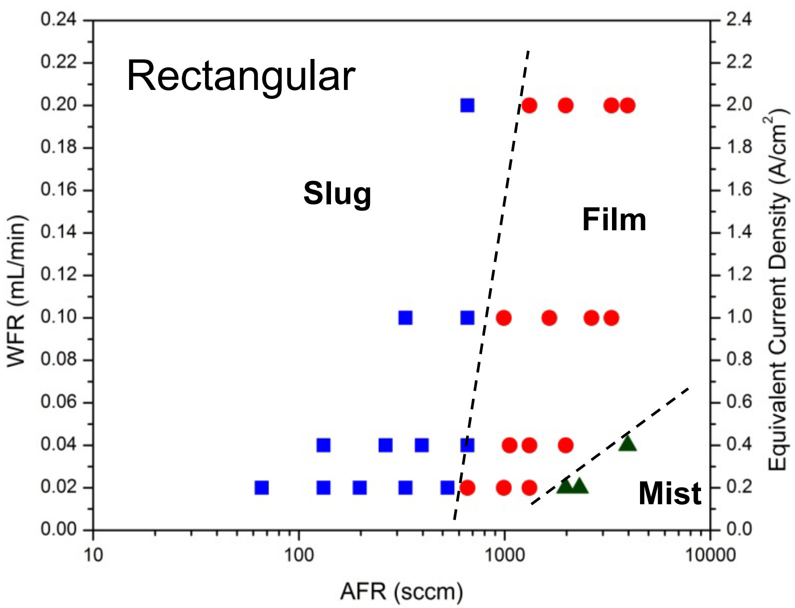

- Trapezoidal and rectangular channels show similar flow structures and flow pattern maps.
- Sinusoidal channels promote more smaller slugs at low air flow rates and more film flow at higher flow rates than the other profiles.

Effect of GDL Thickness on Water Transport Dynamics in Channel

Ex-situ Multichannel Exp.

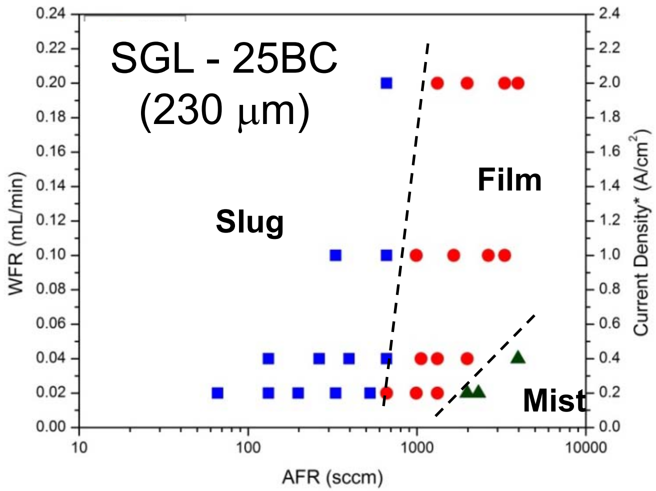

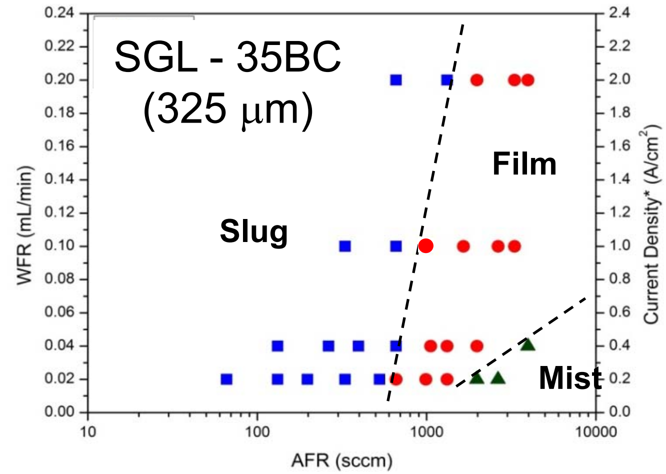

In-situ Multichannel Exp.

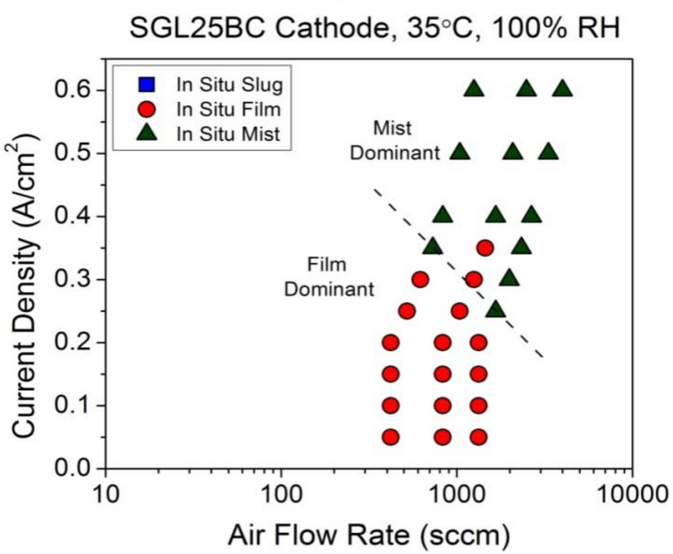

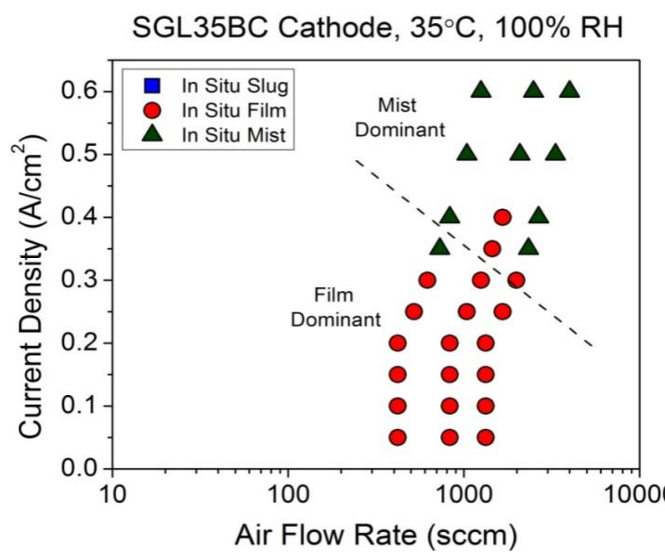

- GDL thickness has insignificant effect on water transport dynamics in channels.

GDL Thermal Conductivity Measurement

- GDL thermal conductivity measured with guarded hot plate method.
- Numerical calculation:

$$R_{Total} = \frac{\Delta T}{\left(Q/_2\right)} = R_{th} + R_c \qquad R_{th} = \frac{L}{k\,A}$$

  - At constant compression and for thickness L_1 and L_2:

$$k = \frac{L_1 - L_2}{(R_{Total1} - R_{Total2})\,A}$$

Guarded hot plate method

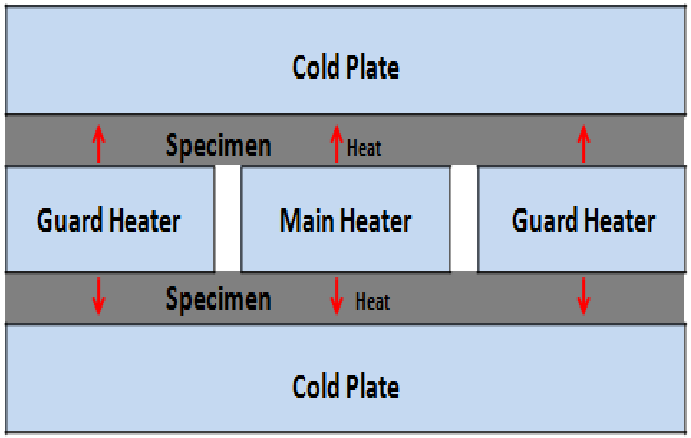

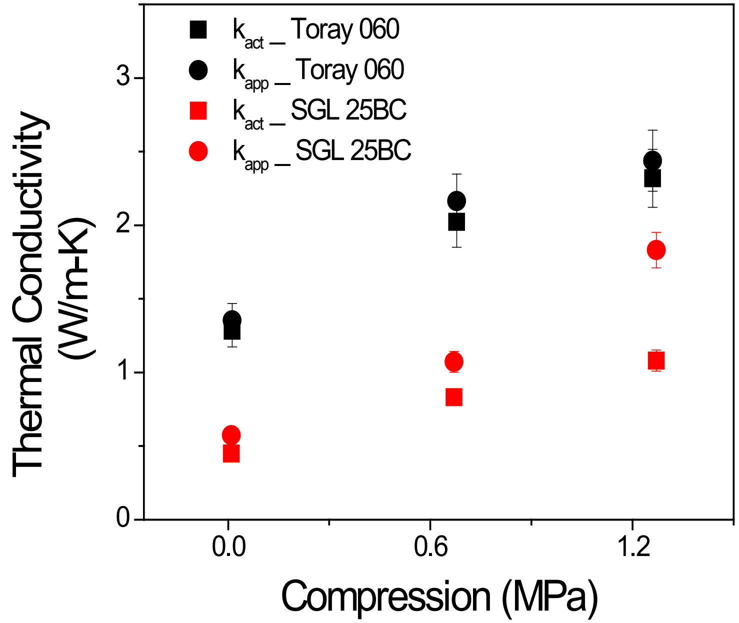

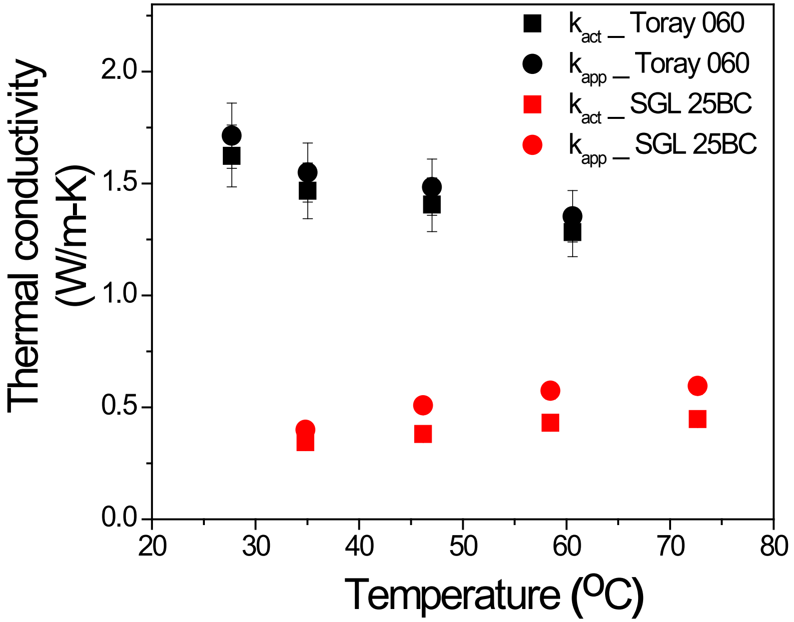

Experimental Determination of Water Vapor Diffusivity in GDL

Experimental Measurement

- Inlet and outlet humidity and temperature precisely controlled.

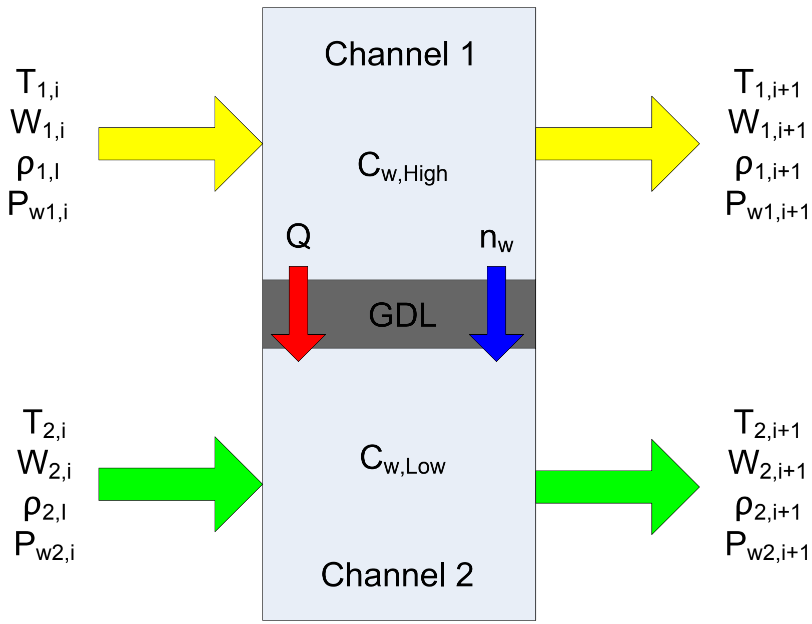

40°C Isothermal Results

Flow rate (slpm)	D ($\times 10^{-4}$ m²/s)
Experimental:	
0.5	0.098
1.0	0.108
1.5	0.107
Average	0.104
Literature value:	
Unrestricted	0.26
Bruggemann correction [a]	0.186
Improved correction [b]	0.139

[a] $$D_{AB}^{eff} = \varepsilon^{1.5} D_{AB}$$

[b] $$D_{AB}^{eff} = D_{AB}\frac{\varepsilon}{\tau}$$

Technical Accomplishments (MTU)–

GDL Wettability Characterization

- ❑ Method developed for accurate measure of contact angle, θ, on rough surfaces (GDL)
- ❑ Temperature control (up to 100°C)
- ❑ Humidity control
- ❑ As temperature increases, θ decreases

Environmental chamber for measuring contact angles

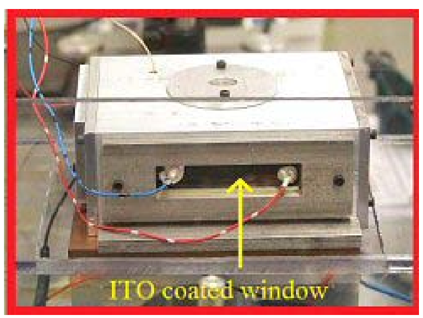

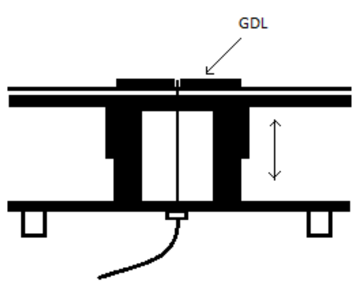

Injection of water drop through GDL for dynamic contact angle measurements.

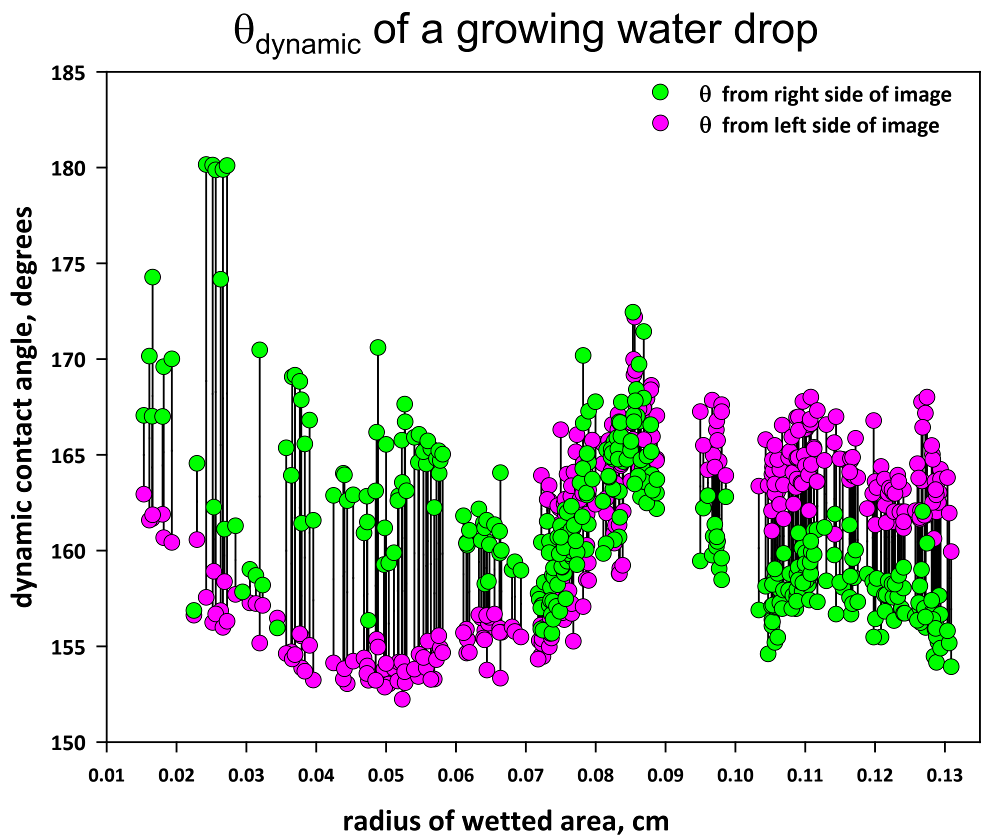

GDL Morphology Characterization

- ❑ Statistical analysis from SEM images
- ❑ Pore size distributions
  - ○ Weibull distribution
  - ○ Distribution of pore depth, pore roundness, pore orientation, nearest neighbor
- ❑ Relative importance of each parameter on water transport

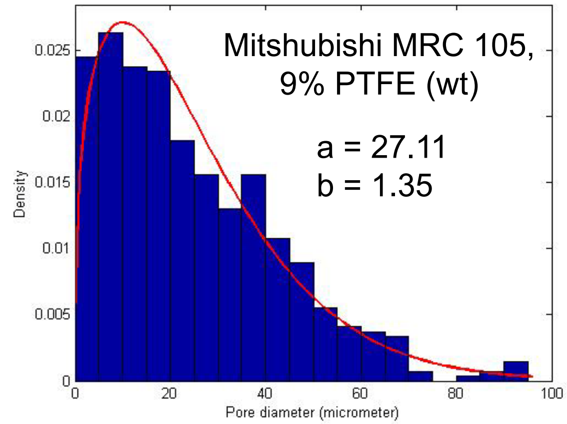

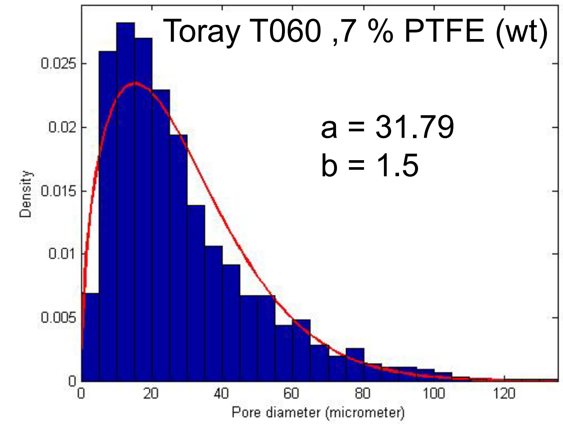

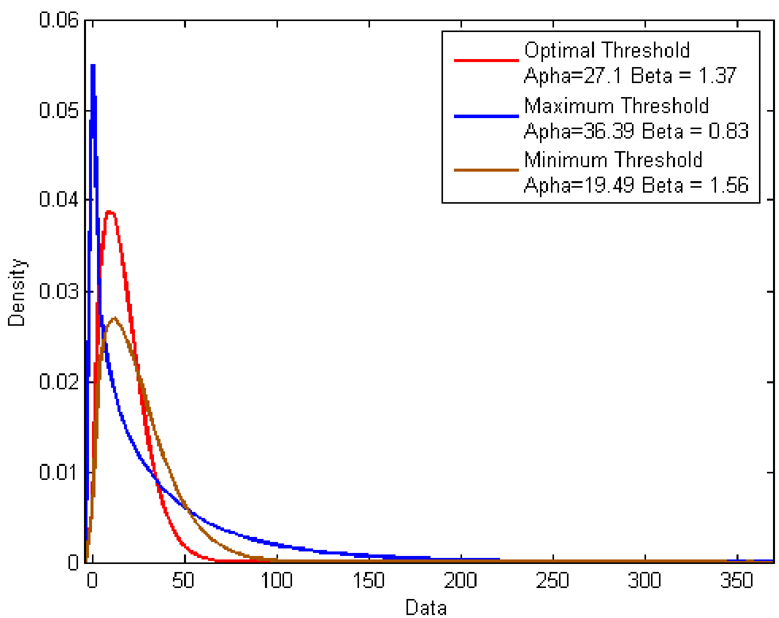

An Otsu algorithm is used to perform histogram shape-based threshhold filtering.

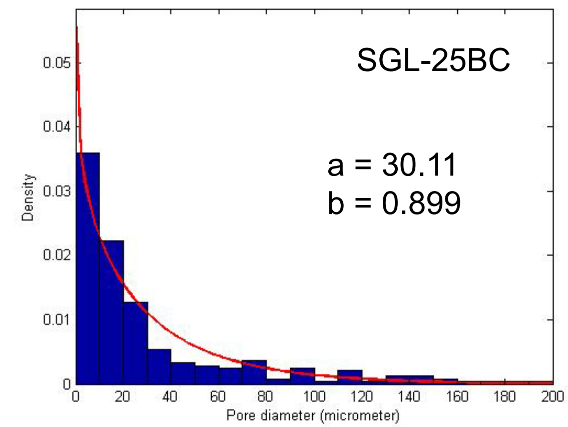

- ❑ Rapid analysis of important GDL parameters – pore size, shape, depth, and orientation distributions.

Existence of Phase Drainage Diagram

Stable Displacement

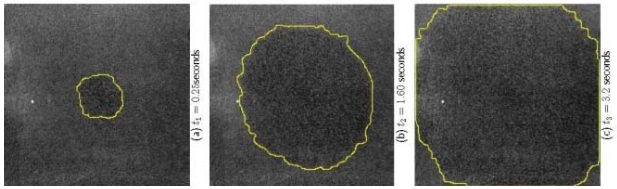

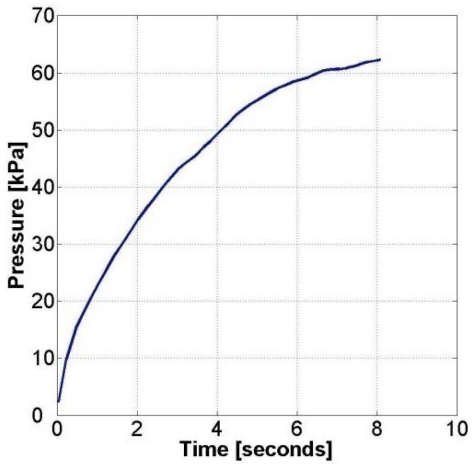

Capillary Fingering

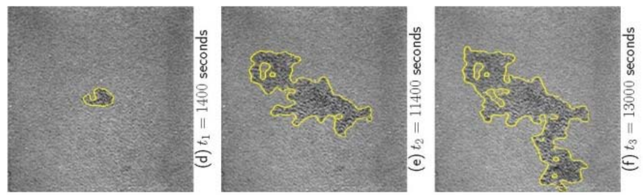

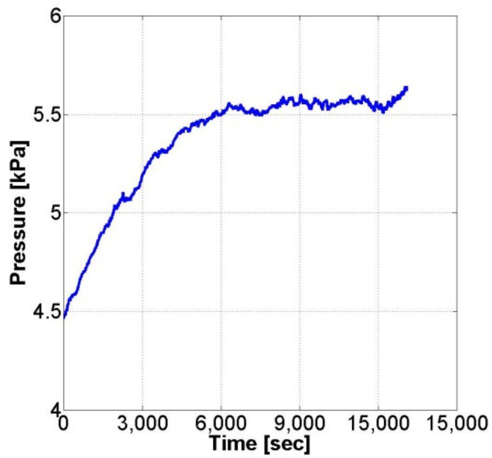

Viscous Fingering

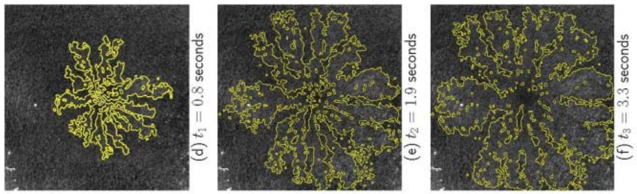

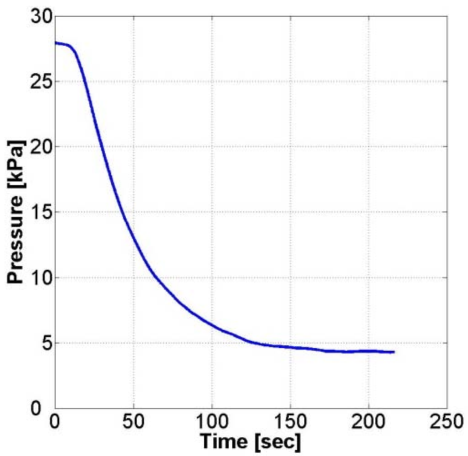

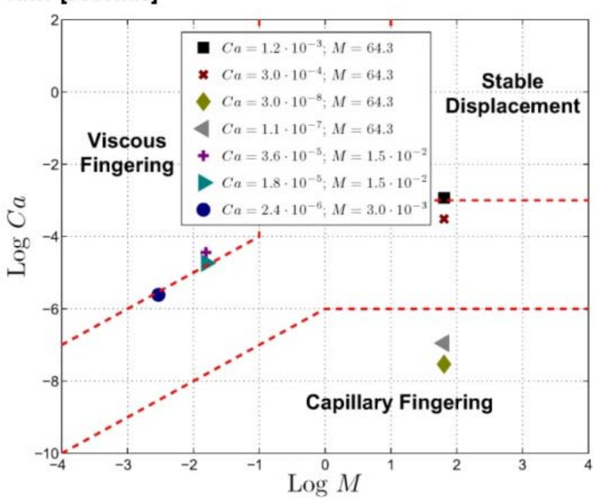

Ca for a typical fuel cell:

$$Ca \approx 10^{-8} - 10^{-9}$$

$$M = \frac{\mu_1}{\mu_2} \qquad Ca = \frac{v\mu_2}{\gamma}$$

Pore Network Model

- ❑ Model inputs:
  - ○ Contact angle (from Wettability studies)
  - ○ Pore size distribution (from Morphology studies)
- ❑ Unique phase drainage diagram for each GDL
- ❑ Unique capillary pressure curve for each type of displacement and GDL

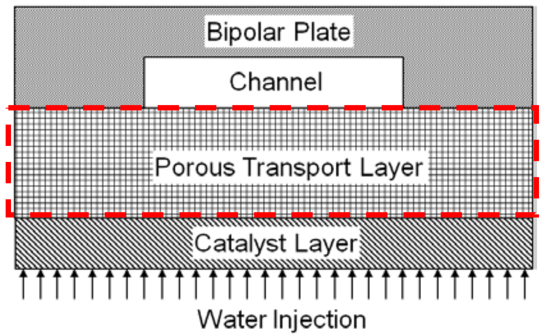

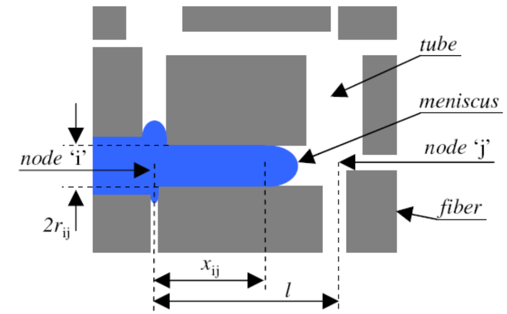

$$\frac{\pi}{8\ell}\sum_{j=1}^{4}\frac{r_{ij}^4}{\mu_{ij}^e}\left(\Delta p_{ij}-p_{ij}^c\right)=0$$

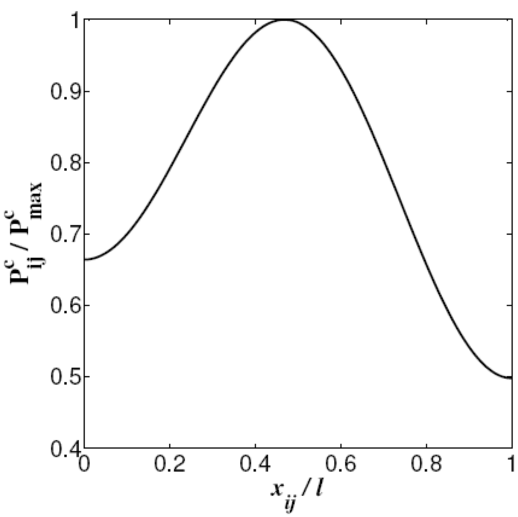

capillary pressure model:

$$p_{ij}^c=\gamma\cos(\theta)\left[\left(1-\frac{r_i}{2\overline{r}_i}-\frac{r_j}{2\overline{r}_j}\right)\frac{1-\cos(2\pi x_{ij}/\ell)}{r_{ij}}+\frac{1+\cos(\pi x_{ij}/\ell)}{\overline{r}_i}+\frac{1-\cos(\pi x_{ij}/\ell)}{\overline{r}_j}\right]$$

- ❑ Simple network model captures dynamics of capillary fingering. The model for the capillary pressure in a pore includes the effect of contact line pinning by allowing the capillary pressure to reach a maximum. The end pressures are the average of the pressures in the four tubes that define a node.

Dynamic GDL Saturation

GDL without MPL

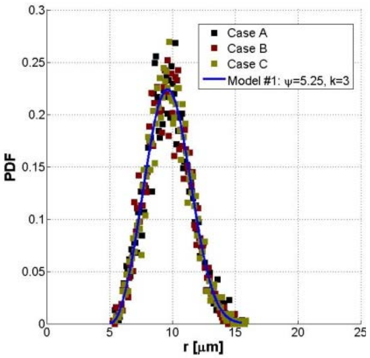

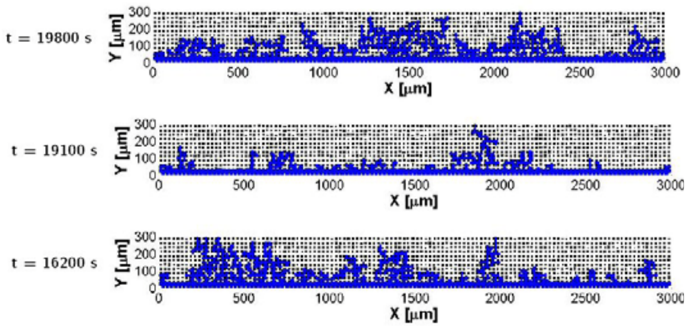

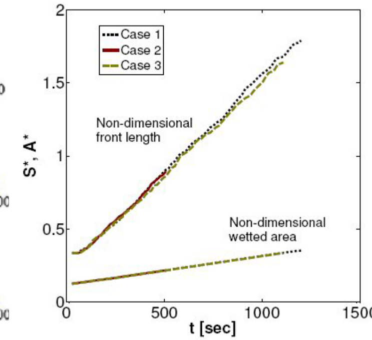

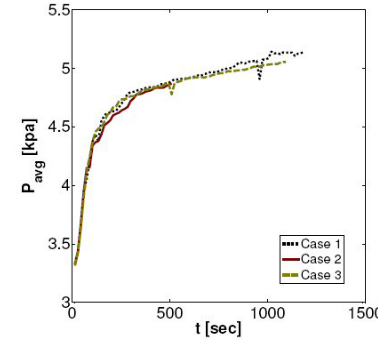

GDL with MPL

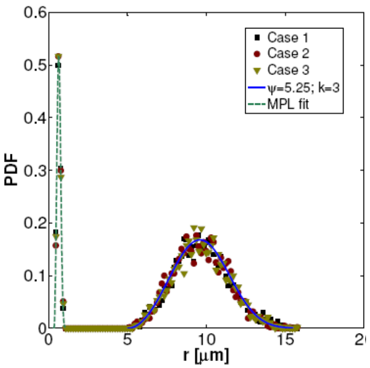

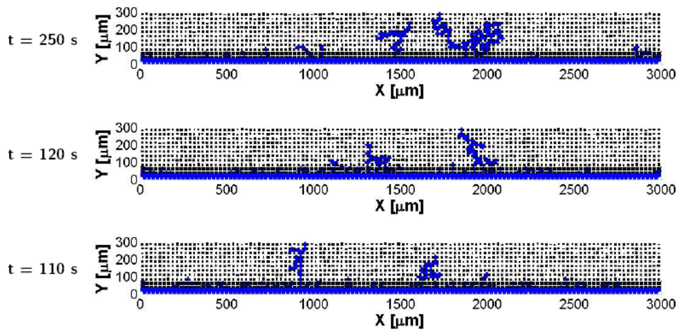

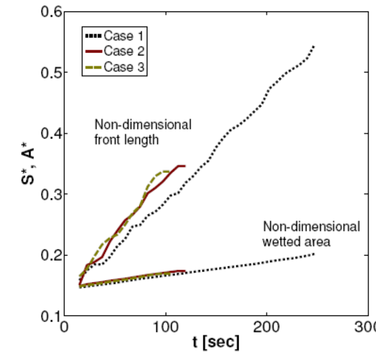

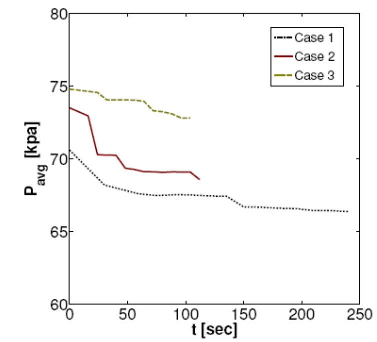

GDL with cracked MPL

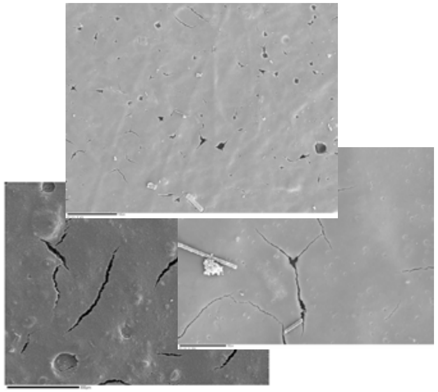

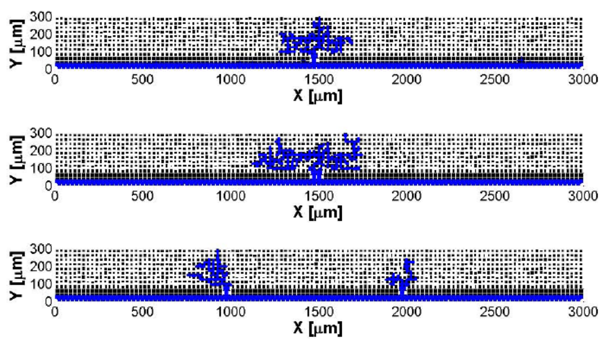

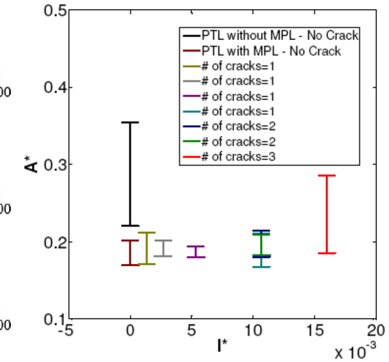

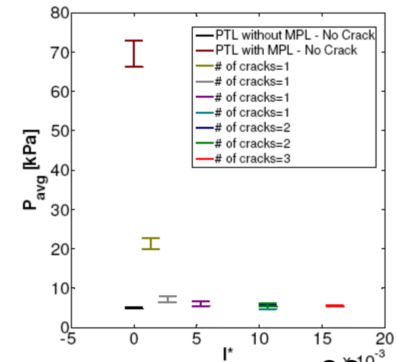

3D Network Model

3D Simulation

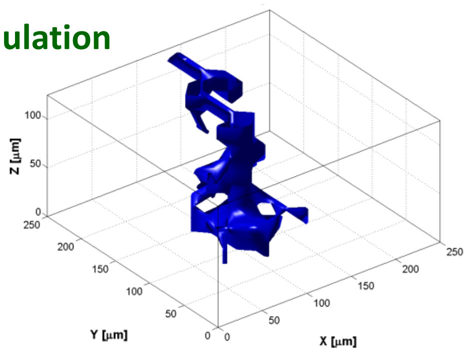

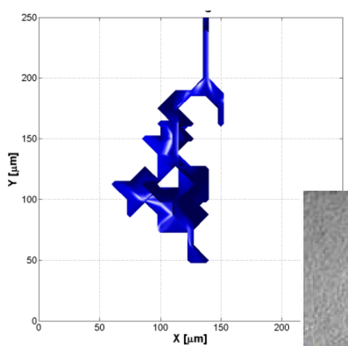

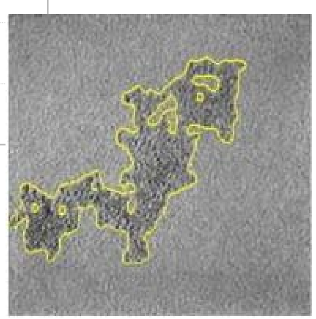

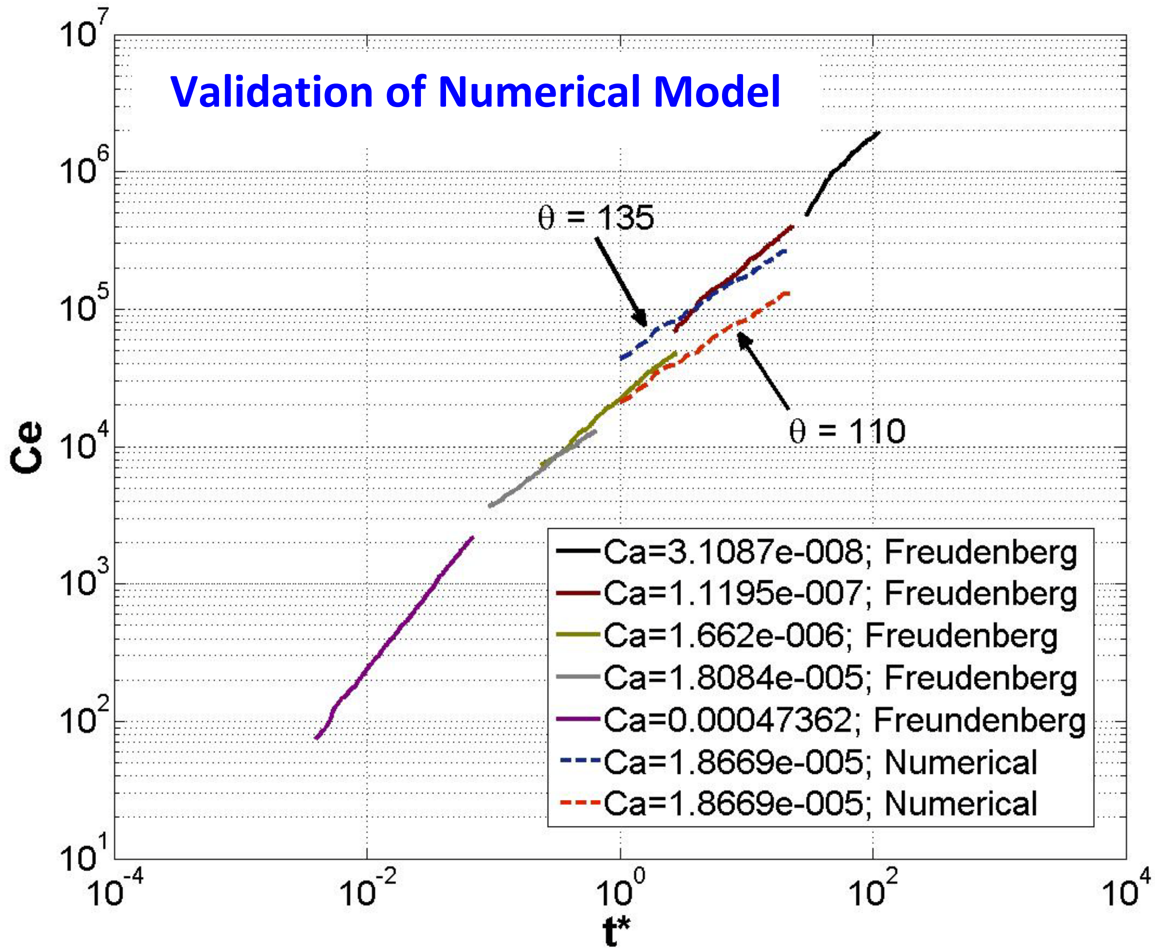

- ❑ Simple Hele-Shaw experiments capture physics of water transport.
- ❑ The network model can accurately predict liquid water transport in GDLs.

Channel Characterization

- The critical plug volume V_{CR} is the minimum liquid volume necessary for a plug to exist. V_{CR} is a function of the wall contact angle θ, the base contact angle θ_{base} and the channel bend opening (dihedral angle).

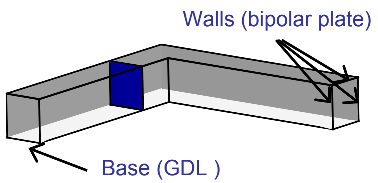

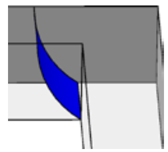

θ = 110°

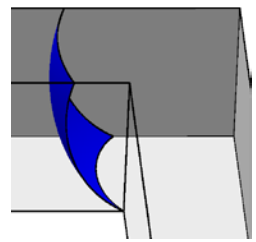

θ = 120°

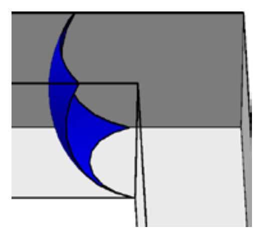

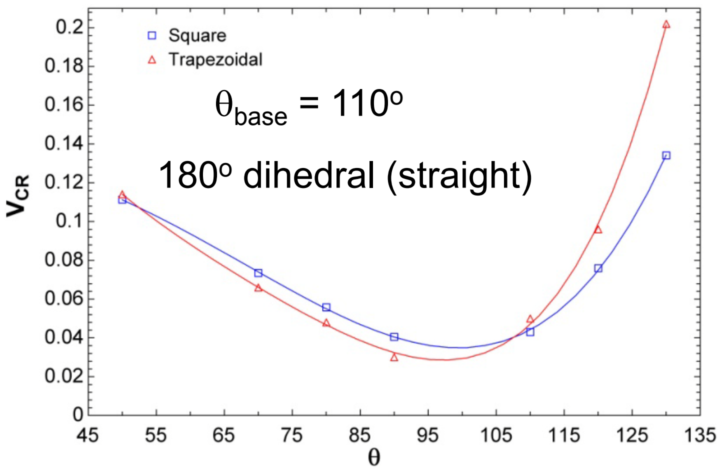

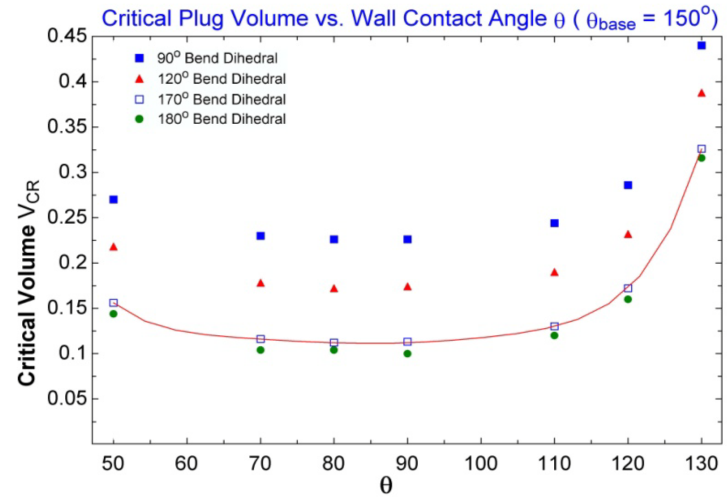

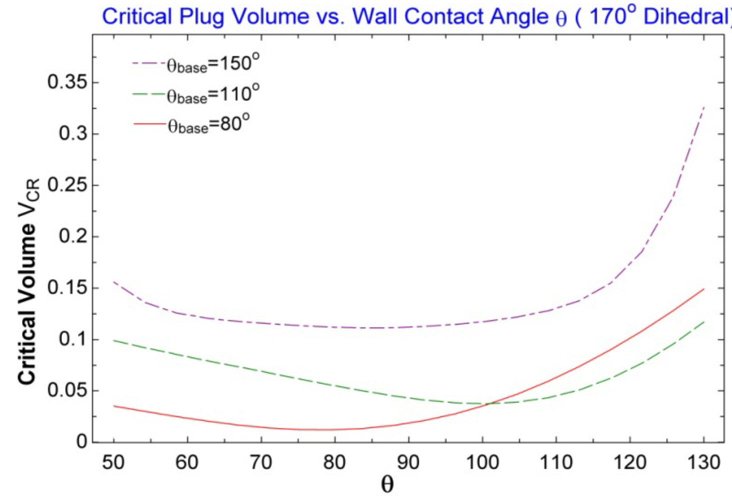

Design considerations for channel holdup optimization:

- Three times more water to form a plug for θ_{base} = 150° than for 110°.
- Effects of surface degradation: V_{CR} will decrease by a factor of 10 if θ_{base} = 150° & θ = 100° degrades to θ_{base} = 80° & θ = 80°..

Summary and Recommendations

❑ Material Set

❖ GDL materials:

- Lower thermal conductivity reduces water accumulation in the GDL due to the increased temperature gradient across the MEA.
- GDL morphology and the pore size distribution in GDL play an important role in water distribution.
- GDL wettability/contact angle depend on droplet size.

Recommendation: use lower thermal conductivity GDL and decrease the anode GDL thickness.

❖ Gas Channel:

- Determined the flow patterns and pressure drop characteristics in gas channels.
- Determined the minimum volume for slug formation in various channel geometries.
- Demonstrated that the hydrophilic channel facilitates the removal of liquid water by capillary effects and by reducing water accumulation at the channel exit.
- Demonstrated that different channel geometries (sinusoidal, trapezoidal and rectangular) have insignificant effects on flow dynamics in channel.

Recommendation: use high production channel geometry with a hydrophilic coating.

Summary (cont'd)

❑ Shutdown purge protocol:

- Found that most of the water accumulation at the shutdown is retained on the anode side.
- Found that GDL ageing produces no significant change in water hold-up or purge effectiveness.
- Found that drying front behavior during purge causes uneven ionomer drying.
- Built a database with locally resolved current, HFR, liquid water, and temperature measurements.

Recommendation: incorporate above findings in developing cost effective and energy efficient shutdown purge protocol.

❑ Water transport mechanism:

- Experimentally established that the purge process can be modeled as a 1D constant rate drying process.
- Modeling of water transport in fuel cell:
  - ➢ Developed a network model to simulate capillary-driven two-phase flow in GDL, with the pore size distributions being modeled by using Weibull distribution functions. The effect of the inclusion of the microporous layer in the fuel cell assembly was explored numerically.
  - ➢ Developed an accurate drying rate model for the drying process in GDL.
  - ➢ A model developed for contact angle variation with temperature and GDL surface structure.
  - ➢ A model developed for water vapor diffusivity through GDL and water retention in the channels

Supplemental Slides

Collaborations

RIT:

- RIT, GM: Development and Integration of Novel Materials for Hydrogen Fuel Cells Applications: experimental study of water generation and transport in gas diffusion media, NYSERDA , February 2008 – May 2009

MTU:

- MTU: Hydrogen Education Curriculum Path at Michigan Technological University, DOE DE-FG36-08GO18108
- MTU, State of Michigan: Fuel Cell Water Control System Prototype – Alternative Energy, Michigan Universities Commercialization Initiative (MUCI)
- VirginiaTech, U. Louisiana-Lafayette, Purdue, MTU: Micro-Hydroforming Processes for Enhancement of PEM Fuel Cell Water Management and Component Manufacturing (NSF Proposal 0900435)
- MTU: Center for Fundamental and Applied Research in Nanostructured and Lightweight Materials (CNLM), DOE DE-FG36-08GO88104

GM:

- NIST: "Partnership for Neutron Imaging of Fuel Cells," December 2008 - December 2009.